minerals

MDPI

Article

Petrogenesis of Serpentinites and Chromitites in the Neoproterozoic Bou Azzer Ophiolite, Morocco: From Mantle Depletion to High-Pressure Exhumation

Amina Wafik [1], Mohamed Ben Massoude [1], Youssef Atif [2], Atman Ait Lamqadem [3], Reza Rooki [4], Aref Shirazi [5,*], Adel Shirazy [5,6,*] and Amin Beiranvand Pour [7,8]

1 Excellence Research Laboratory Aquabiotech, GeoSciences Semlalia-Team Geology Department, Faculty of Sciences Semlalia, Cadi Ayyad University, Marrakech 40000, Morocco; wafik@uca.ac.ma (A.W.); benmassoud.20@gmail.com (M.B.M.)
2 Laboratory of Geosciences, Environment and Related Resources (GERA), Department of Geology, Faculty of Sciences Dhar El Mahraz, Sidi Mohamed Ben Abdellah University, Atlas Fez B.P. 1796, Morocco; atifyoussef6@gmail.com
3 Laboratory of Geodynamic and Geomatics, Department of Geology, Faculty of Sciences, Chouaïb Doukkali University, El Jadida 24000, Morocco; aitlamqadem.a@ucd.ac.ma
4 Department of Mining Engineering, Birjand University of Technology, Birjand 9719866981, Iran; rooki@birjandut.ac.ir
5 Department of Mining Engineering, Amirkabir University of Technology, Tehran 1591634311, Iran
6 Karlsruhe Institute of Technology (KIT), Kaiserstraße 1276131, Karlsruhe Campus Nord, Her-Mann-Von-Helmholtz-Platz 1, 76344 Eggenstein-Leopoldshafen, Germany
7 Institute of Oceanography and Environment (INOS), Universiti Malaysia Terengganu (UMT), Kuala Nerus 21030, Terengganu, Malaysia; beiranvand.pour@umt.edu.my
8 School of Earth Sciences, Damghan University, Damghan 3671641167, Iran
* Correspondence: aref.shirazi@gmail.com (A.S.); adel.shirazy@gmail.com (A.S.); Tel.: +98-9121877608 (A.S.); +98-9121506256 (A.S.)

Abstract

Serpentinites and associated chromitites of the Neoproterozoic Bou Azzer ophiolite (Central Anti-Atlas, Morocco) provide key constraints on mantle depletion, melt–rock interaction, and the tectono-metamorphic evolution of a supra-subduction zone (SSZ) system. This study integrates field observations, petrography, Raman spectroscopy, and whole-rock/mineral chemistry to decipher the history of this highly dismembered ultramafic suite. The mantle sequence is dominated by antigorite-bearing serpentinites derived primarily from refractory harzburgitic and dunitic protoliths. Whole-rock geochemistry and highly depleted chromite compositions (Cr# = 0.50–0.68; Mg# = 0.43–0.77; $TiO_2 \leq 0.18$ wt.%) demonstrate that these peridotites represent refractory residues formed after high degrees of partial melting (~15–25%). The data delineate a clear evolutionary trend from abyssal to fore-arc and back-arc environments, where infiltrating boninitic melts drove localized podiform chromitite formation through intense melt–rock interaction. Crucially, thermodynamic and mineral–chemical constraints challenge previous models of simple greenschist-facies obduction. Equilibration temperatures exceeding 600 °C and chromite stability within the lower amphibolite to near-granulite facies indicate that the oceanic lithosphere underwent deep subduction prior to its exhumation. This high-temperature, high-pressure metamorphism was followed by multistage retrogressive serpentinization and intense CO_2-rich metasomatism (talc-magnesite alteration) during Pan-African transpressional tectonics. Ultimately, the Bou Azzer ophiolite represents a mature SSZ mantle wedge, recording a complete geodynamic cycle from deep subduction-zone metamorphism to final tectonic emplacement along the northern margin of the West African Craton.

Academic Editors: Andrei Y. Barkov and Robert F. Martin

Received: 12 March 2026
Revised: 8 April 2026
Accepted: 14 April 2026
Published: 29 April 2026

Keywords: Bou Azzer; neoproterozoic ophiolite; serpentinites; podiform chromite; SSZ mantle wedge; Pan-African orogeny

1. Introduction

Neoproterozoic ophiolitic complexes provide critical tectonic windows into the evolution of the oceanic lithosphere during the assembly of Gondwana. They are essential for understanding fundamental processes such as mantle melting, melt extraction, and supra-subduction zone dynamics [1,2]. In this context, the Bou Azzer inlier, located in the Central Anti-Atlas of Morocco, represents a classic Pan-African ophiolitic massif. It is widely recognized as a key site for investigating the Neoproterozoic oceanic lithosphere and its subsequent obduction onto the West African Craton (WAC) [3–10].

The Bou Azzer ophiolite consists of a dismembered, tectonically disrupted sequence comprising mantle peridotites, mafic-ultramafic cumulates, sheeted dikes, pillow lavas, and an associated accretionary mélange [11,12]. This assemblage is intruded by syn- to post-kinematic calc-alkaline granitoids and is unconformably overlain by Ediacaran volcanic and sedimentary cover [11]. The tectonic history of the massif is well-constrained, involving two major Pan-African phases (B1 and B2) characterized by folding, metamorphism, and faulting [7,13,14]. More recent studies identify at least three deformation phases—D1 (early convergence and thrusting), D2 (collisional thickening), and D3 (late transcurrent to transtensional tectonics with post-collisional magmatism) [7,15–17]. Structurally, the ophiolite is interpreted as an obducted sequence with a basal mélange, showing high-temperature (HT) greenschist-facies metamorphism (≈5–6 kbar, 500–550 °C) [18].

Despite this well-defined tectonic framework, the specific geodynamic setting of the mantle protolith remains debated. Geochemical discrimination is essential to resolve this, particularly by estimating the degree of partial melting. Abyssal peridotites are generally interpreted as residual products of moderate mantle melting (<20%) resulting from decompression beneath mid-ocean spreading centers [19–21]. In contrast, Supra-Subduction Zone (SSZ) peridotites represent highly depleted rocks formed in the sub-arc region, characterized by high degrees of partial melting (approx. 15% to 40%) [22].

However, applying these distinctions to Bou Azzer is challenging due to extensive serpentinization, which obscures primary mineralogy [10,12,23]. Although significant research has focused on the tectonic setting of the Bou Azzer serpentinites [10,23,24], there is still little information available regarding the precise mantle magmatic processes and their geochemical evolution. To bridge this gap, systematic variations in whole-rock geochemistry and the composition of relict chromian spinel must be utilized to trace the melt depletion history [25,26].

In this paper, we present new petrographic data, mineral chemistry (with a focus on chromian spinel), and whole-rock geochemistry of serpentinites and associated chromitites from the Bou Azzer ophiolite. The primary objective is to constrain the nature of the mantle protolith (Abyssal vs. SSZ), evaluate the extent of fluid/melt–rock interactions, and refine the geodynamic model for the Neoproterozoic mantle evolution beneath the West African Craton.

2. Geological Setting

The Anti-Atlas belt, situated in southern Morocco (Figure 1a), forms the northern boundary of the West African Craton (WAC). It consists of a vast anticlinorium exposing Paleoproterozoic basement inliers and Neoproterozoic assemblages, unconformably overlain by a thick Paleozoic sedimentary cover [27]. The chain is structurally divided by the Major

Anti-Atlas Fault (MAAF), a major tectonic lineament separating the belt into two domains (Figure 1b): the Western Anti-Atlas, dominated by the Eburnean cratonic basement, and the Central to Eastern Anti-Atlas, where Neoproterozoic Pan-African terrains are extensively exposed [3,4,13,14,27,28].

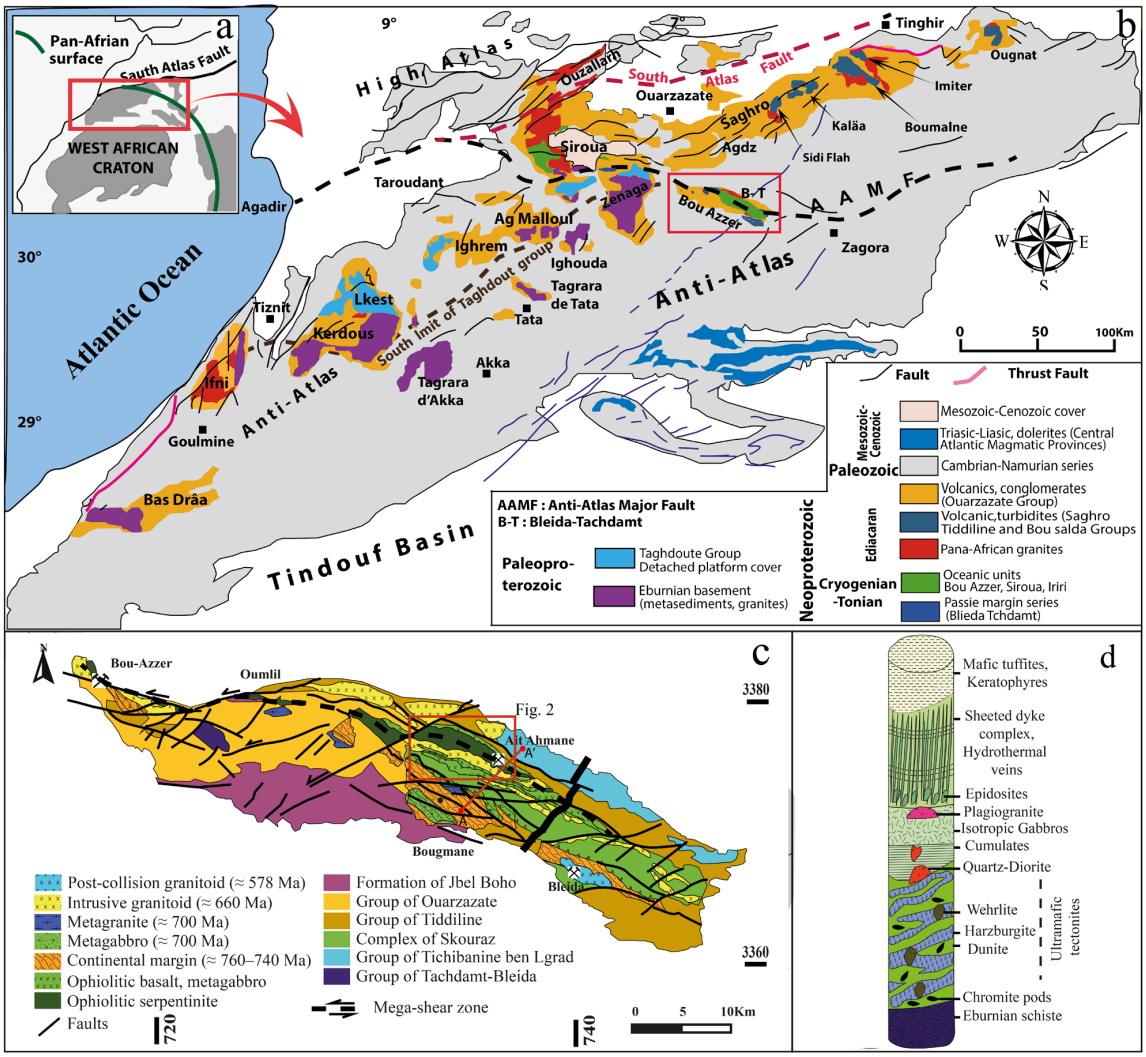

Figure 1. (**a**) Schematic map showing the location of the Anti-Atlas orogenic belt at the northern boundary of the WAC. (**b**) Simplified geological map of the Anti-Atlas (modified after Gasquet et al. [29], and Soulaimani et al. [17]. The red rectangle indicates the position of the Bou Azzer inlier. (**c**) Detailed geological map of the Bou Azzer inlier displaying the main lithotectonic units—including continental margin sequences, ophiolitic and arc associations, and syn- to post-tectonic granitoids—as well as the location of mining districts. Modified after Leblanc [12], Oberthür et al. [30], and Blein et al. [31], as compiled by Wafik et al. [9]. (**d**) Synthetic stratigraphic column of the Bou Azzer ophiolite illustrating the main lithostratigraphic units, adapted from Wafik et al. [9].

The region records a complex polycyclic history. The Paleoproterozoic Eburnean orogeny (≈2 Ga) produced the cratonic basement [32,33]. However, the current architecture is primarily the result of the Neoproterozoic Pan-African orogeny, which drove the formation of volcanic arc complexes and ophiolitic sequences in the Central Anti-Atlas [3,14,34,35]. While the domain was later affected by Variscan shortening [14] and localized Alpine reactivation [36], the fundamental lithostructural framework of the inliers remains Pan-African.

The Bou Azzer-El Graara inlier is located in the Central Anti-Atlas, along the MAAF, approximately 45 km southwest of Ouarzazate (Figure 1b,c). It represents a erosional inlier into the Pan-African suture zone, exposing a collage of oceanic and arc-related terranes.

The basement comprises Tonian to early Cryogenian Formations (900–700 Ma) attributed to the Tachdamt-Bleida and Tazzegzout Group [7,37,38]. These are spatially associated with two Cryogenian arc systems (Figure 1c): the Northern Arc (Tichibanine-Ben Laghlad Group): A tectonic assemblage of metagreywackes, basalts, andesites, rhyolites, and tuffs, dated between 761 ± 7 Ma and 767 ± 7 Ma [5,31,38,39], and the Southern Arc (Bougmane-Bou Azzer Group), composed mainly of orthogneiss, metagabbro, and pegmatites [7,31,40].

The Bou Azzer ophiolite marks the suture resulting from the northward subduction of the oceanic crust (~760 Ma) and its subsequent obduction onto the WAC margin [7,16,41]. The sequence is highly dismembered and consists of serpentinized mantle peridotites hosting podiform chromitites, layered gabbros, sheeted diabase dykes, and pillow lavas associated with oceanic sedimentary rocks [3,4,12–14,28,42] (Figure 1a–d).

Magmatic activity in the inlier concluded with late- to post-orogenic intrusions. The ophiolitic and arc assemblages are crosscut by syn-orogenic quartz-diorite intrusions dated at 660–640 Ma [31,38,43,44] and essentially undeformed post-orogenic gabbro-diorites dated at 594 ± 1.2 Ma [31,45].

3. Analytical Methods

This study is based on a representative set of serpentinites and associated lithologies collected from the Bou Azzer ophiolite. Sampling was conducted on surface outcrops, exploration trenches, and diamond drill cores (SC06, SC08, and SC09) to cover the various facies of the ultramafic sequence. A total of 40 samples were selected for petrographic analysis, and polished thin sections were prepared at the Faculty of Sciences Semlalia (Cadi Ayyad University, Marrakech, Morocco).

Petrographic observations were carried out using standard optical microscopy (transmitted and reflected light). Complementary mineral characterization was conducted using Micro-Raman spectroscopy (Cadi, Ayyad University, Marrakesh, Morocco) on thin sections, utilizing a SOL Instruments Confotec MR 520 equipped with a 532 nm laser source. Micro-textures were imaged using a Tescan VEGA3 Scanning Electron Microscope (SEM) at the Centre of Analysis and Characterization (CAC), Cadi Ayyad University. The SEM is equipped with a high-resolution panchromatic Cathodoluminescence (CL) detector (185–850 nm) and a silicon drift Energy Dispersive Spectrometer (EDS) for qualitative chemical analysis. Analyses were performed under an accelerating voltage of 20 kV and a beam current of 15 nA.

Quantitative chemical compositions of primary (chromian spinel) and secondary minerals (serpentine group) were determined using Electron Probe Micro-Analysis (EPMA). Analyses were carried out at two facilities: the Service Commun de Microscopies Électroniques et de Microanalyses X at Lorraine University (Nancy, France) using a JEOL JXA-8800, and the Department of Petrology and Mineralogy at Paris VI University (Jussieu, France) using a Camebax microprobe. Both instruments operated in Wavelength Dispersive Spectrometry (WDS) mode. Analytical conditions were set at an accelerating voltage of 15 kV, a probe current of 20 nA, and a beam diameter of 3 µm. Counting times were typically 10 to 20 s per element. Calibration was performed using natural and synthetic standards, and data were corrected using standard ZAF procedures.

Whole-rock geochemical analyses were performed at the REMINEX Laboratories (Managem Group, Casablanca, Morocco). Samples were crushed and pulverized to a fine powder (<75 µm). Major element concentrations were determined by Atomic Emission

Spectrometry (ICP-AES) following total acid dissolution. A multi-acid digestion procedure ($HF–HNO_3–HClO_4$) was employed to ensure the complete dissolution of refractory mineral phases. Data quality was monitored through the analysis of certified international reference materials (CRMs) and procedural blanks.

4. Results

4.1. Lithology and Field Relations

The Bou Azzer inlier is characterized by abundant serpentinite bodies, representing the mantle section of the Neoproterozoic ophiolitic complex. These rocks generally outcrop as WNW–ESE-trending belts, forming steeply dipping sheets or lenses emplaced along major thrust faults (Figure 2). They are spatially associated with a lithological assemblage comprising ultramafic cumulates, layered metagabbros, and schistose metavolcanic rocks. Derived from the hydrothermal alteration of peridotitic protoliths (mainly harzburgites and dunites), the serpentinites show distinct tectonic contacts with the surrounding mafic units (gabbros, microgabbros, and quartz diorites). This contact is well-exposed, dipping 60–80° to the north, and is locally delineated by a reactional alteration halo.

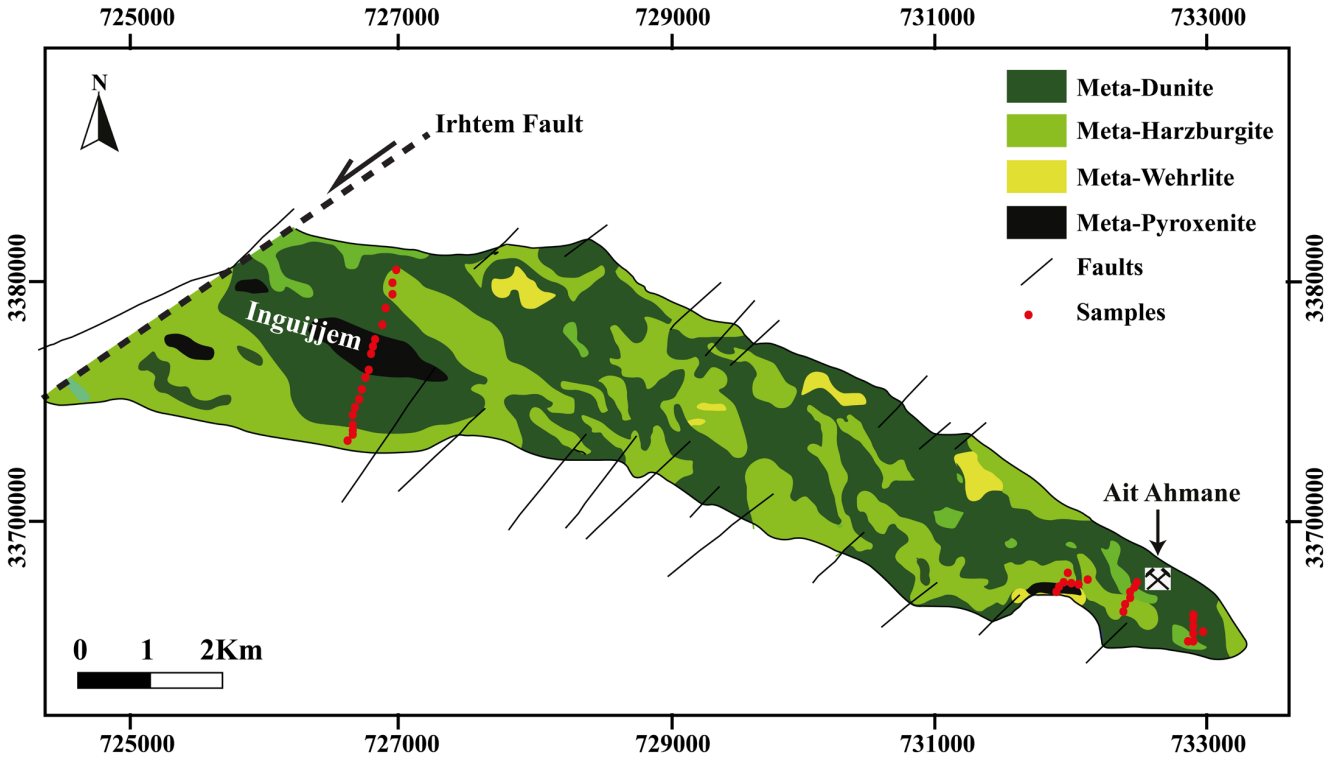

Figure 2. Geological map of Ait Ahmane Inguijem ultramafic tectonites.

Structurally, the serpentinites are cut by two main fracture sets: (i) subhorizontal fractures oriented N130°/20°SW, and (ii) subvertical fractures trending N190°/60°NW. Magnetite is ubiquitous, occurring either as fine disseminations or as fracture fillings forming pockets up to 5 cm in diameter.

Figure 3 highlights the structural complexity of the Aït Ahmane–Inguijem sector. In the general view (Figure 3a), massive serpentinites and intercalated metagabbro–diabase bodies dominate the foreground. A striking angular unconformity is observed between the Adoudounian limestones and the underlying Neoproterozoic rhyolites (Ouarzazate Group), testifying to the region's polyphase tectono-sedimentary evolution. Along the northwestern margin, the serpentinite body shows a sharp contact with the overlying "green rocks" (Zone D), spatially coincident with the cobalt-bearing mineralization.

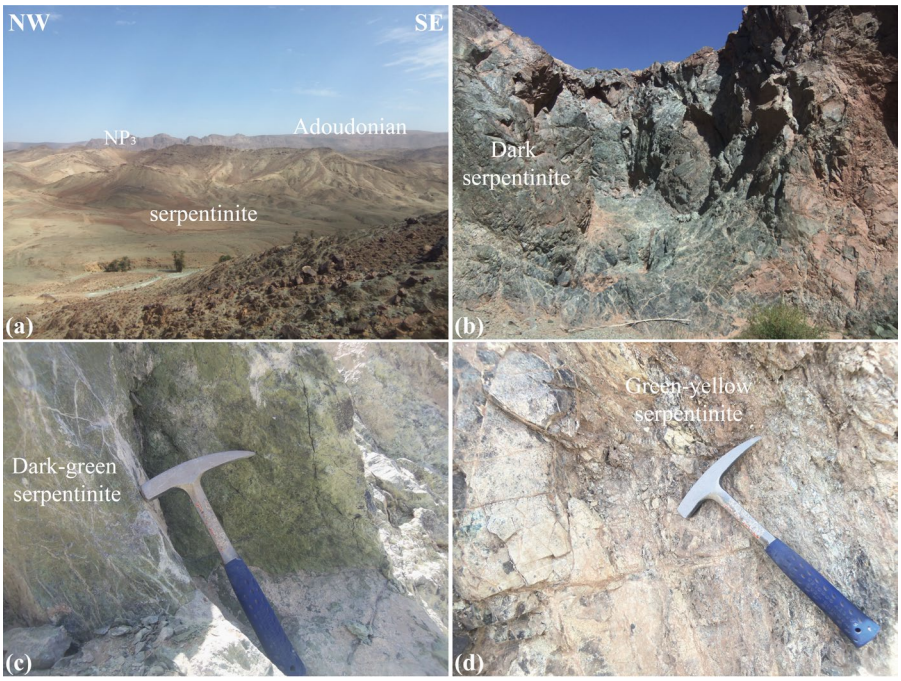

Figure 3. Field photographs illustrating the Aït Ahmane–Inguijem ophiolitic sequence. (**a**) Panoramic view of the ophiolitic imbricates, dominated by massive serpentinites and metagabbro–diabase associations in the foreground. Note the prominent angular unconformity (discordance) between the overlying Adoudounian limestones and the Neoproterozoic rhyolites of the Ouarzazate Group. (**b**–**d**) Detailed views of the different serpentinite facies, showing the complete replacement of the peridotitic protolith.

At the macroscopic scale (Figure 3b–d), surface outcrops are completely serpentinized, yet distinct facies can be distinguished based on color and texture:

Green serpentinites: Interpreted as serpentinized harzburgites with a preserved tectonite texture. They outcrop as discontinuous bands parallel to the structural axis.

Green-yellow serpentinites: Corresponding to serpentinized dunites, typically occurring as lenses.

Dark serpentinites: Rare facies, possibly derived from serpentinized wehrlites, exhibiting a massive aspect.

While surface rocks are fully altered, drill core data and local observations indicate that primary lithologies (gabbros and rare dunites) are preserved at depth. In high-strain zones associated with major faults, the serpentinites are frequently transformed into talc-schists, carbonated serpentinites, or listvenites, characterized by intense shearing and dense networks of chrysotile veinlets.

Chromitite pods in the Bou Azzer–El Graara boutonnière occur as lenticular bodies (cm to >50 m) within fully serpentinized peridotites, aligned mainly at N110°E–N130°E. They are concordant or locally discordant to L1. Chromite content increases from harzburgites (<5%) to massive chromitites (>95%), with lizardite–dolomite–chromite assemblages. For more details, see [24,46].

4.2. Petrography and Mineralogy

Combined petrographic observations, Raman spectroscopy, and SEM imaging reveal that the ultramafic rocks are extensively serpentinized, composed primarily of antigorite, lizardite, and chrysotile, with minor magnetite, chromian spinel, carbonates, and talc. The integration of these methods allows for the distinction of three main textural types corresponding to specific serpentine polymorphs (Figures 4 and 5).

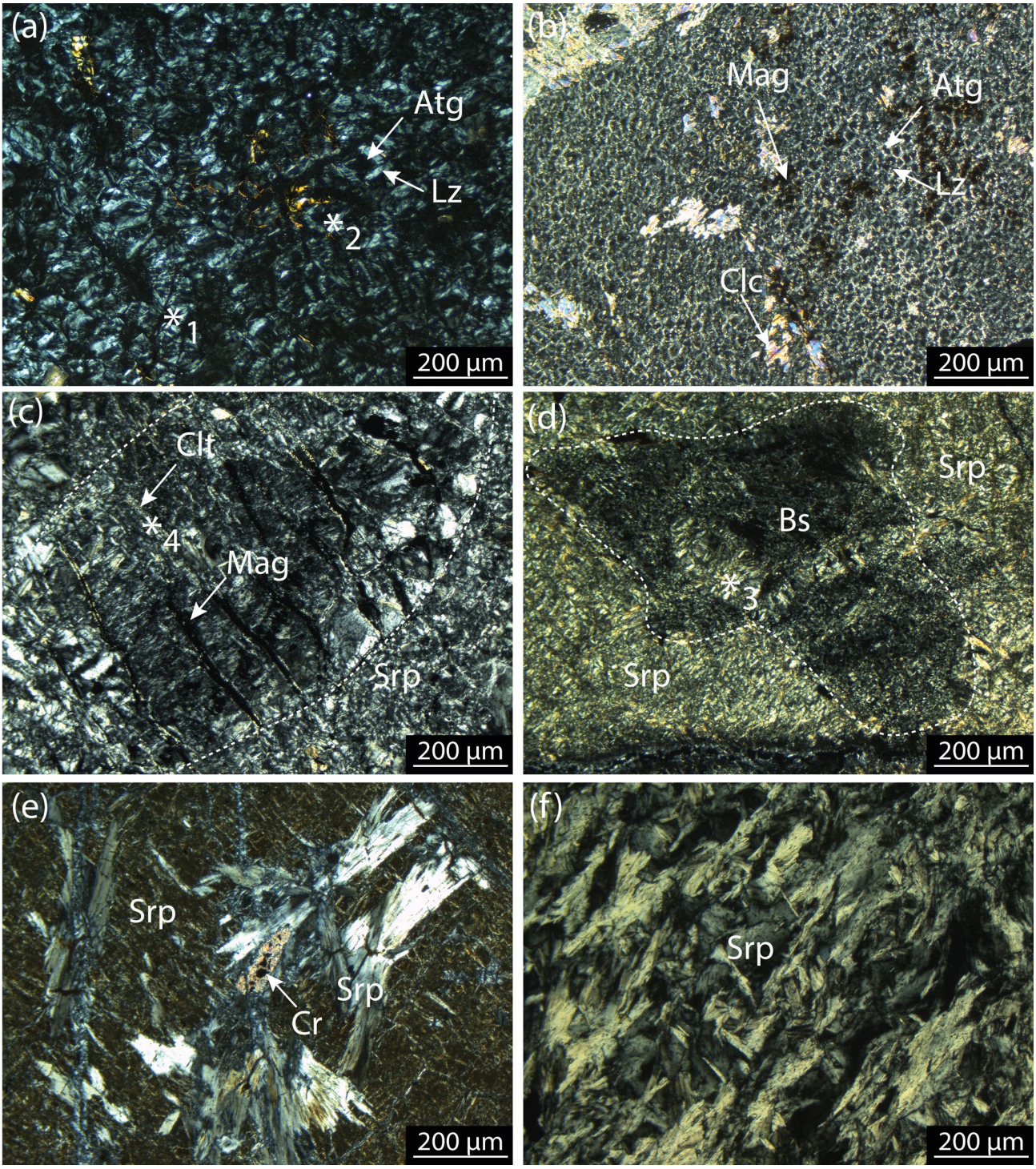

Figure 4. Photomicrographs of the Bou Azzer serpentinites showing characteristic textures. (**a**,**b**) Fully serpentinized dunite displaying mesh textures resulting from the complete replacement of olivine. Note the characteristic "hourglass" extinction patterns and late-stage clinochrysotile veins crosscutting the matrix. (**c**,**d**). Serpentinized harzburgite exhibiting bastite pseudomorphs after orthopyroxene, associated with fibrolamellar textures and a dense network of secondary veins. (**e**,**f**) Deformed serpentinite illustrating the progressive replacement of pseudomorphic mesh textures by plumose and interlocking (interpenetrating) textures. Magnetite veins typically outline microfractures and surround relict mesh cores. Atg: antigorite; Bs: Bastite; Cr: Chromite; Clt: chrysotile; Lz: lizardite; Mag: magnetite; Srp: serpentine; Clc: Clinochlore. *1,*2, *3, *4 indicate Raman analysis location in Figure 5.

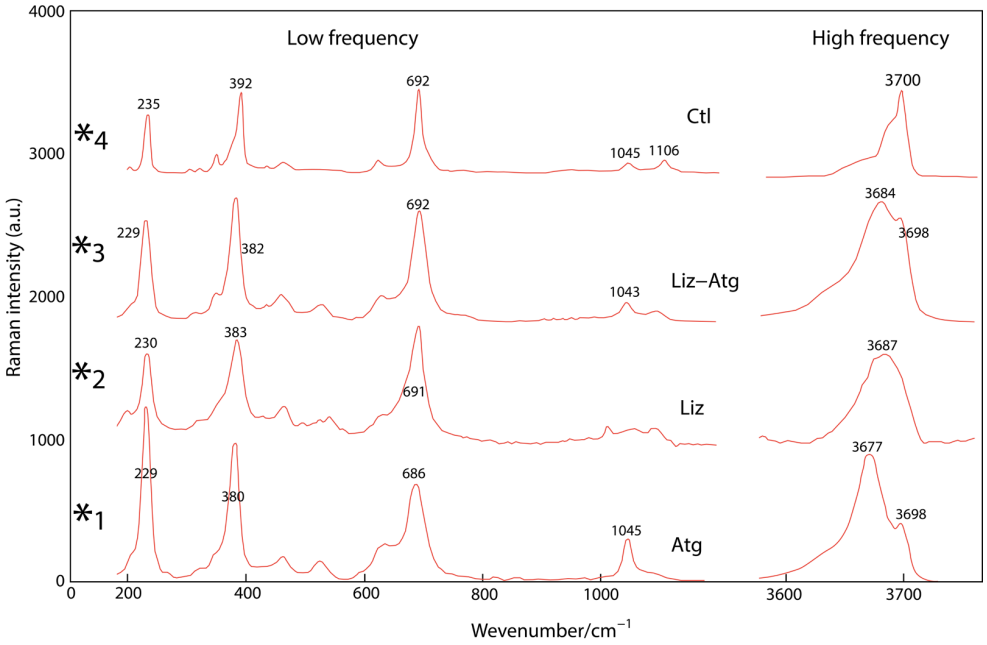

Figure 5. Transmitted Representative Raman spectra of the serpentine polymorphs (antigorite, lizardite, and chrysotile) identified in the Bou Azzer ultramafic rocks. The spectra display two distinct domains: the low-frequency region (150–1150 cm^{-1}), characteristic of lattice modes and Si–O vibrations, and the high-frequency region (3600–3720 cm^{-1}), corresponding to O–H stretching vibrations. Spectral band assignments are based on Schwartz et al. [47]. *1,*2, *3, *4 indicate Raman analysis location in Figure 4.

In massive and less deformed facies (metadunites and metaharzburgites), original cumulus textures are partially preserved. Olivine is replaced by lizardite forming characteristic mesh textures with "onion-skin" or hourglass patterns (Figure 4a,b). Orthopyroxene is replaced by bastite (lizardite), which preserves the original cleavage (Figure 4c,d). Raman spectroscopy confirms the identification of lizardite in these domains, exhibiting characteristic bands at ~382 and ~690 cm^{-1}, with a sharp OH-stretching peak around ~3686 cm^{-1} (Figure 5). SEM images show that lizardite crystals are predominantly prismatic (Figure 6). In these textures, excess iron expelled during serpentinization forms magnetite rims outlining the pseudomorphs or filling fractures.

In sheared and foliated samples, the primary mesh and bastite textures are obliterated and replaced by interlocking, interpenetrating, or ribbon-like textures (Figure 4e,f). These domains are dominated by antigorite, which is spectrally distinguished by a prominent Raman band near ~1045 cm^{-1} and an OH-stretching vibration at ~3677 cm^{-1} (Figure 5). Mixed Raman spectra (Lizardite + Antigorite) are commonly recorded, reflecting the progressive metamorphic overprinting of early lizardite by antigorite in high-strain zones.

The matrix is invariably crosscut by late-stage veins of fibrous chrysotile, clinochlore, and talc (Figure 4b,c). SEM imaging highlights that these fibrous phases overprint both mesh and bastite textures, indicating they represent the latest serpentine generation (Figure 6). Raman analysis of these veins reveals a broader spectral signature with bands near ~1110 cm^{-1} and distinctive OH-stretching peaks between ~3649 and 3700 cm^{-1}.

Chromian spinel is the only relict magmatic mineral, although it is commonly fractured and rimmed by secondary "ferritchromite" and magnetite (see Figure 4). Idiomorphic magnetite is ubiquitous, occurring either as fine disseminations within the serpentine mesh or as macroscopic veinlets.

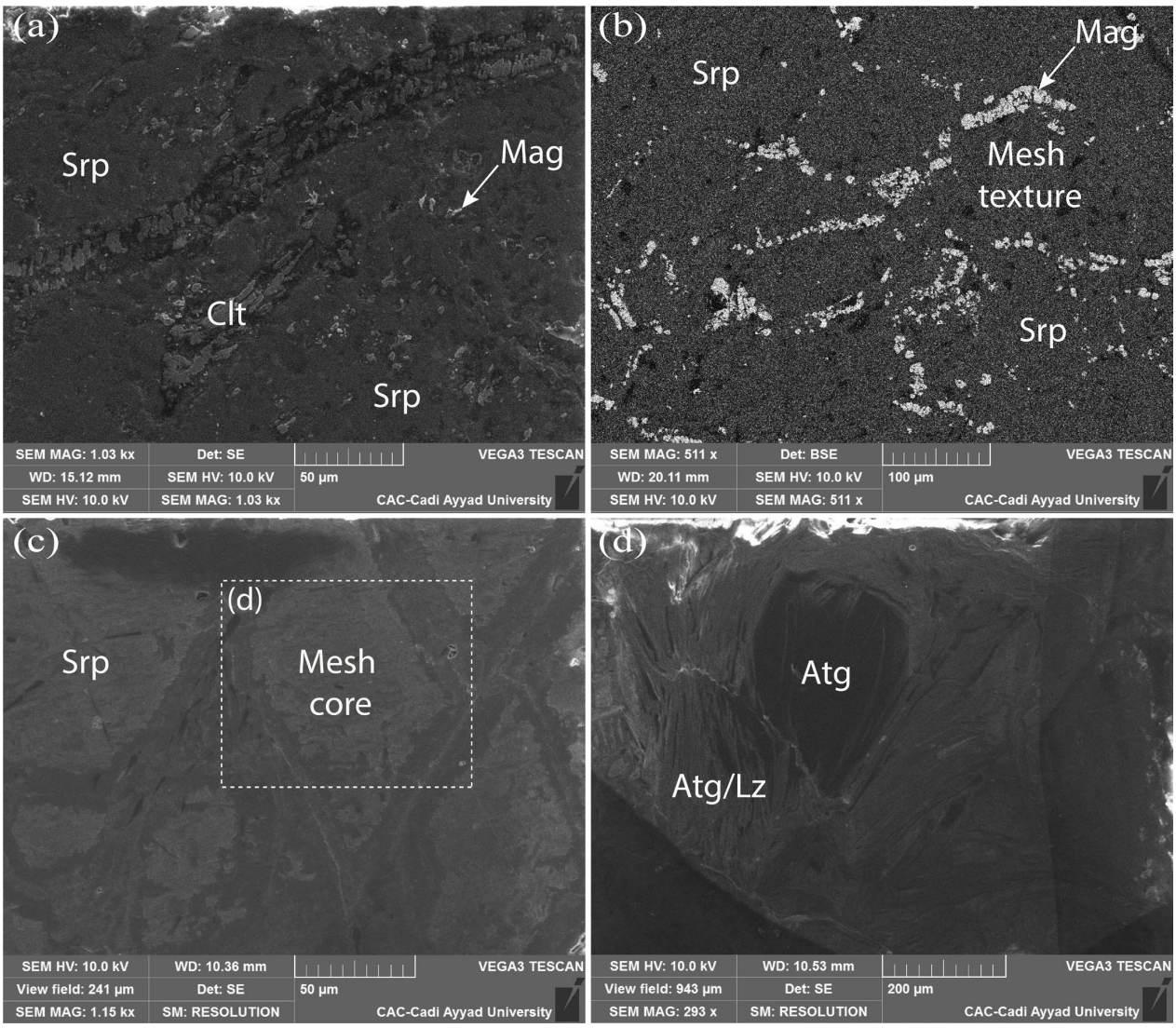

Figure 6. Secondary Electron (SE) and Back-Scattered Electron (BSE) images illustrating the textural evolution and mineral replacements in the Bou Azzer serpentinites. (**a**) Development of ribbon textures and microfracture-related domains crosscutting the primary mesh network, marking the transition toward serrate veins. (**b**) Fully pseudomorphic mesh texture (lizardite) exhibiting grey cores and dark rims, associated with needle-like magnetite. (**c**) Characteristic mesh texture developed after olivine. (**d**) Progressive textural evolution showing the replacement of initial mesh textures by interlocking and interpenetrating textures (antigorite). Mineral abbreviations: Atg: antigorite; Clt: chrysotile; Lz: lizardite; Mag: magnetite; Srp: serpentine.

Tables 1–3 summarize the key geochemical characteristics of the analyzed samples. The weight loss on ignition (LOI; Table 1) ranges from 5.11 to 23.67 wt.%, indicating near-complete serpentinization. Table 2 represents CIPW normative mineral compositions and calculated petrogenetic parameters of the Bou Azzer serpentinized peridotites. Table 3 represents trace element composition in Bou Azzer serpentinites.

The serpentinites exhibit significant hydration, with LOI values generally ranging from 5.1 to 14.6 wt.%, and reaching up to 23.7 wt.% in highly altered samples (e.g., BB 20). Despite this pervasive alteration, the geochemical signature of the protolith remains identifiable.

The rocks are characterized by low SiO_2 (typically 30.2–44.4 wt.%) and high MgO concentrations (30.7–42.3 wt.%). This results in high MgO/SiO_2 ratios (0.8–1.0) and high Mg# (Mg/[Mg + Total Fe]) ranging from 0.81 to 0.85, consistent with a refractory mantle origin (dunite to harzburgite).

In the majority of samples, immobile elements such as Al_2O_3 and TiO_2 are very low (<1.5 wt.% and <0.05 wt.%, respectively), confirming the depleted nature of the mantle sequence. Na_2O and K_2O contents are negligible (<0.05 wt.%), typical of abyssal or fore-arc peridotites.

Calcium concentrations are generally extremely low (<0.1 wt.%) in the preserved serpentinites, reflecting the leaching of clinopyroxene during partial melting and subsequent serpentinization. However, specific samples (e.g., ST2, BMAA 5a) exhibit high CaO values (up to 22 wt.%), which correlate with the presence of secondary carbonate phases (calcite/dolomite) or localized calcic metasomatism.

Table 1. Whole-rock major element compositions (wt.%) and Loss on Ignition (LOI) of the Bou Azzer serpentinites.

Sample	SiO_2	Al_2O_3	Fe_2O_3	CaO	MgO	TiO_2	Co	Cr	Ni	LOI (%)
BA 11	32.1	0.37	11.4	3.77	30.7	0.01	140	7790	1820	20.65
BA 12	37.4	0.29	13.3	0	34.3	0.01	461	2460	2500	13.7
J 010	53.9	7.43	10.4	3.92	17.9	0.29	71	2070	506	5.16
J 07	40.8	0.26	4.59	0	38.7	0.01	74	3040	2120	14.64
ST 1	41.3	0.58	8.06	3.34	40.49	0.01	148	2348	2235	5.22
ST 2	36.82	0.38	6.69	8.11	37.44	0.01	101	2209	2004	9.55
ST 3	39.97	0.21	5.91	0.82	38.52	0.01	127	2445	1771	13.56
SA	39	0.43	7.68	3.31	38.64	0.01	144	2027	2059	9.93
AA BH 1	40.58	1.02	6.88	0.64	40.73	0.01	116	2179	2280	9.14
AA BH 2	43.14	1.08	5.87	0.69	41.22	0.01	185	2774	2189	6.99
AA BH 4	43.06	1.01	5.82	0.69	40.26	0.02	106	2060	1730	8.14
AA BH 5	43.07	0.34	3.8	0.98	42.32	0.01	135	2379	2405	8.48
AA BH 6	41.17	1.15	6.82	2.85	37.45	0.01	97	2114	2231	9.55
AA BH 7	42.22	0.51	5.91	0.56	40.4	0.01	108	1862	2054	9.39
AA BH 9	44.38	0.3	5.56	0.85	38.08	0.01	122	1768	2162	9.82
BB 14	42.41	0.99	7.08	1.73	41.66	0.02	118	2082	1964	5.11
BB 16	54.04	2.28	5.31	1.84	29.46	0.05	75	1024	1416	6.02
BB 20	30.19	1.75	8.71	2.18	31.46	0.04	141	4509	4080	23.67
BMAA 105	38.9	1.04	2.2	0.34	39.71	0.02	18	1418	1242	14.4
BMAA 5a	34.85	12.99	11.35	22.06	9.46	0.49	44	256	127	8.8
BMAA 5b	41.19	1.03	5.5	0.28	35.43	0.01	14	1214	1125	13.03
BMAA 14	40.61	0.99	3.03	0.52	37.79	0.01	<8	1841	1780	13.44
BMAA 35	35.19	0.6	7.81	0.38	39.82	0.01	27	2329	1897	13.54
BMAA 52	36.89	1.5	8.93	0.27	35.43	0.02	64	2195	2095	13.19
BMAA 109	40.2	0.56	7.59	0.32	32.85	0.01	53	1622	1630	12.85
BM I1	39.82	0.22	6.59	0.43	37.16	0.01	38	1632	1850	13.17
BM I2	46.38	1.04	6.27	0.27	29.23	0.01	<8	1215	1260	12.07

Table 2. CIPW normative mineral compositions and calculated petrogenetic parameters of the Bou Azzer serpentinized peridotites. Normative abundances are calculated from whole-rock major element chemistry and expressed in volume percent (vol.%). DI: Differentiation Index; Est. $T_l$iq (°C): Estimated liquidus temperature, °C; Est. H_2O (wt.%): Estimated H_2O content, wt.%. Mg#: Mg/(Mg + Total Fe) in rock; $Fe^{3+}/\Sigma Fe$: Fe^{3+}/(Total Fe) in rock.

Sample	Rock	Plagioclase (Anorthite)	Diopside	Hypersthene	Olivine	Larnite	Ilmenite	Magnetite	Chromite	Total	$Fe^{3+}/\Sigma Fe$	Mg#	Mg/ (Mg + Fe^{2+})	DI	Est. $T_l$iq (°C)	Est. H_2O (wt.%)
BA 11	Dunite	1.13			86.41	6.13	0.02	4.44	1.88	100	12	72.7	75.2	1.1	1471	0.11
BA 12	Harzburgite			13.11	81.25		0.02	4.77	0.55	100	12	71.9	74.4		1423	0.1
J 010	Orthopyroxenite	18.55		70.25			0.53	3.51	0.43	100	12	63	66	24.9	1171	0.57
J 07	Harzburgite			35.13	62.02		0.02	1.8	0.74	100	12	89.3	90.5		1289	0.2
ST 1	Dunite	1.48	11.73	1.51	81.77		0.02	2.77	0.5	100	12	83.3	85	1.7	1382	0.1
ST 2	Dunite	1.08	0.1		83.22	12.62	0.02	2.43	0.5	100	12	84.7	86.3	1.1	1425	0.1
ST 3	Harzburgite	0.53	3.11	22.97	70.34		0.02	2.26	0.58	100	12	86.6	88	0.7	1326	0.14
SA	Wehrlite	1.07	12.06		83.11	0.22	0.02	2.78	0.45	100	12	83.3	85	1.3	1386	0.1
AA BH 1	Harzburgite	2.74	0.39	15.97	77.58		0.02	2.49	0.49	100	12	85.4	87	3	1357	0.11
AA BH 2	Harzburgite	2.96	0.33	25.71	68.12		0.02	2.09	0.61	100	12	87.4	88.8	3.1	1320	0.15
AA BH 4	Harzburgite	2.74	0.54	28.39	65.43		0.04	2.1	0.46	100	12	87.3	88.6	3	1310	0.16
AA BH 5	Harzburgite (Cpx)	0.92	3.22	26.7	67.02		0.02	1.4	0.54	100	12	91.7	92.6	1	1294	0.18
AA BH 6	Harzburgite (Cpx-rich)	3.21	9.05	14.57	70.02		0.02	2.48	0.48	100	12	84.5	86.1	3.3	1342	0.12
AA BH 7	Harzburgite	1.43	1.07	26.63	68.16		0.02	2.16	0.42	100	12	87.1	88.5	1.5	1317	0.15
AA BH 9	Opx-rich Harzburgite	0.62	2.93	39.45	53.98		0.02	2.05	0.4	100	12	87.2	88.5	1.1	1269	0.23
BB 14	Harzburgite	2.69	4.54	13.41	76.38		0.04	2.45	0.45	100	12	85.4	86.9	2.7	1356	0.11
BB 16	Orthopyroxenite	6.33	2.28	88.91			0.1	1.89	0.23	100	12	84.6	86.2	6.6	1117	0.88
BB 20	Dunite	5.45			87.18	2.21	0.09	3.59	1.15	100	12	78.2	80.3	5.7	1462	0.11
BMAA 105	Harzburgite	2		28.79	67.4		0.04	0.91	0.36	100	12	94.7	95.3	2	1286	0.2
BMAA 5a	Orthopyroxenite	34.24			38.85	22.05	0.9	3.81	0.05	100	12	45.2	48.4	34.2	1498	0.11
BMAA 5b	Harzburgite	1.57		42.08	53.27		0.02	2.17	0.3	100	12	86.5	87.9	1.6	1276	0.21
BMAA 14	Harzburgite	3		37.19	58.05		0.02	1.23	0.46	100	12	92.5	93.3	3	1265	0.24
BMAA 35	Dunite	1.8			94.55	0.06	0.02	2.99	0.55	100	12	83.5	85.2	1.8	1421	0.1
BMAA 52	Harzburgite	1.47		16.55	76.91		0.04	3.41	0.52	100	12	79.7	81.7	1.5	1388	0.1
BMAA 109	Harzburgite	1.73	0.05	40.81	54		0.02	2.99	0.4	100	12	81.1	83	1.7	1296	0.18
BM I 1	Harzburgite	0.67	1.35	27.85	67.19		0.02	2.54	0.39	100	12	84.8	86.4	0.7	1321	0.14
BM I 2	Orthopyroxenite	1.51		79.26	15.84		0.02	2.46	0.29	100	12	82.2	84	1.5	1172	0.57

https://doi.org/10.3390/min16050460

Table 3. Whole-rock trace element concentrations (ppm) of the Bou Azzer serpentinites.

Sample	As	B	Be	Co	Cr	Cu	Fe	Mn	Nb	Ni	Pb	Sn	Ti	Y	Zn
BA 11	204	44	1	140	7790	19,000	92,800	696	0	1820	41	0	60	0	5870
BA 12	432	36	1	461	2460	4950	79,000	1160	0	2500	10	0	540	0	6240
J 010	25	7	1	71	2070	8070	72,738	1081	16	506	95	20	1737	7	129
J 07	<8	8	1	74	3040	47	32,102	309	<1	2120	63	<20	60	<2	40
ST 1	247	172	2	148	2348	69	56,372	1158	17	2235	156	253	60	4	254
ST 2	115	141	2	101	2209	50	46,790	926	13	2004	66	202	60	3	166
ST 3	107	91	2	127	2445	22,459	41,335	1235	15	1771	77	222	60	3	174
SA	514	139	1.9	144	2027	284	53,714	849	14	2059	171	225	60	3	143
AA BH 1	276	70	1.9	116	2179	246	48,119	309	13	2280	205	213	60	4	113
AA BH 2	599	63	1.9	185	2774	163	41,055	772	14	2189	90	245	60	4	74
AA BH 4	527	54	1.8	106	2060	60	40,705	386	27	1730	417	290	120	4	97
AA BH 5	45	29	1.9	135	2379	1721	26,577	849	18	2405	218	234	60	4	50
AA BH 6	42	69	1.9	97	2114	60	47,699	772	16	2231	117	226	60	3	100
AA BH 7	126	52	1.9	108	1862	62	41,335	772	23	2054	580	263	60	3	77
AA BH 9	347	85	1.8	122	1768	44	38,887	695	25	2162	<26	300	60	4	80
BB 14	64	55	1.9	118	2082	29	49,518	926	17	1964	193	225	120	3	78
BB 16	13	43	1.9	75	1024	58	37,138	386	24	1416	63	286	300	5	103
BB 20	215	67	2	141	4509	46	60,918	926	23	4080	384	283	240	4	226
BMAA 105	26	37	<0.2	18	1418	44	15,380	464	39	1242	26	52	119.6	4	40
BMAA 5a	19	98	<0.2	44	256	204	38,500	542	83	127	419	433	59.8	11	718
BMAA 5b	35	63	<0.2	14	1214	43	21,200	696	<1	1125	<26	35	59.8	3	154
BMAA 14	80	58	<0.2	<8	1841	42	54,600	619	<1	1780	27	43	59.8	5	10,446
BMAA 35	24	54	<0.2	27	2329	44	62,500	1390	<1	1897	32	45	119.6	3	192
BMAA 52	10	75	<0.2	64	2195	6	53,100	1	16	2095	34	43	59.8	4	103
BMAA 109	24	86	<0.2	53	1622	78	46,100	619	<1	1630	<26	32	59.8	4	62
BM I 1	26	77	<0.2	38	1632	39	43,800	542	11	1850	3934	39	59.8	2	112
BM I 2	43	74	2.3	<8	1215	56	79,600	1550	<1	1260	<26	156	60	4	77

Due to the absence of primary silicates, the CIPW normative mineralogy was calculated on an anhydrous basis to classify the protoliths (Table 2). The results indicate a dominance of normative olivine (60–95%) and orthopyroxene, classifying the protolith rocks mainly as harzburgites and dunites. Samples with higher normative diopside correspond to lherzolitic or wehrlitic trends, though this often reflects secondary calcification rather than primary modal composition.

Whole-rock trace element concentrations are listed in Table 3 and illustrated in Primitive Mantle-normalized spider diagrams (Figure 7). The analytical data reveal significant geochemical variability across the serpentinite suite, reflecting a complex interplay between the primary refractory mantle signature and secondary overprints.

Calcium concentrations are generally extremely low (<0.1 wt.%) in the preserved serpentinites, reflecting the leaching of clinopyroxene during partial melting. However, specific samples (e.g., ST2, BMAA 5a) exhibit high CaO values (up to 22 wt.%), which correlate with localized calcic metasomatism.

The compatible transition metals (Cr, Ni, Co) display high concentrations typical of refractory mantle residues. Chromium contents are consistently elevated, generally exceeding 1000 ppm and reaching up to 7790 ppm in chromite-bearing facies, which reflects the abundance of accessory chromian spinel. Similarly, Nickel concentrations are characteristic of depleted peridotites, typically ranging between 1200 and 2500 ppm, with local enrichments reaching 4509 ppm in sample BB 20. Cobalt contents, ranging from approximately 40 to 460 ppm, show a positive covariance with nickel and chromium, further supporting a residual mantle origin.

Finally, chalcophile and metallogenic elements (Cu, Zn, As) exhibit extreme variability, highlighting the superposition of a mineralization event upon the background mantle signature. Copper values vary from typical mantle background levels (<50 ppm) to ore-grade concentrations, reaching 19,000 ppm (1.9 wt.%) in sample BA 11. A similar trend is observed for arsenic and zinc, which are notably enriched in specific samples (e.g., 599 ppm As in AA BH 2), spatially correlated with the known Co–Ni–As mineralization system of the Bou Azzer district.

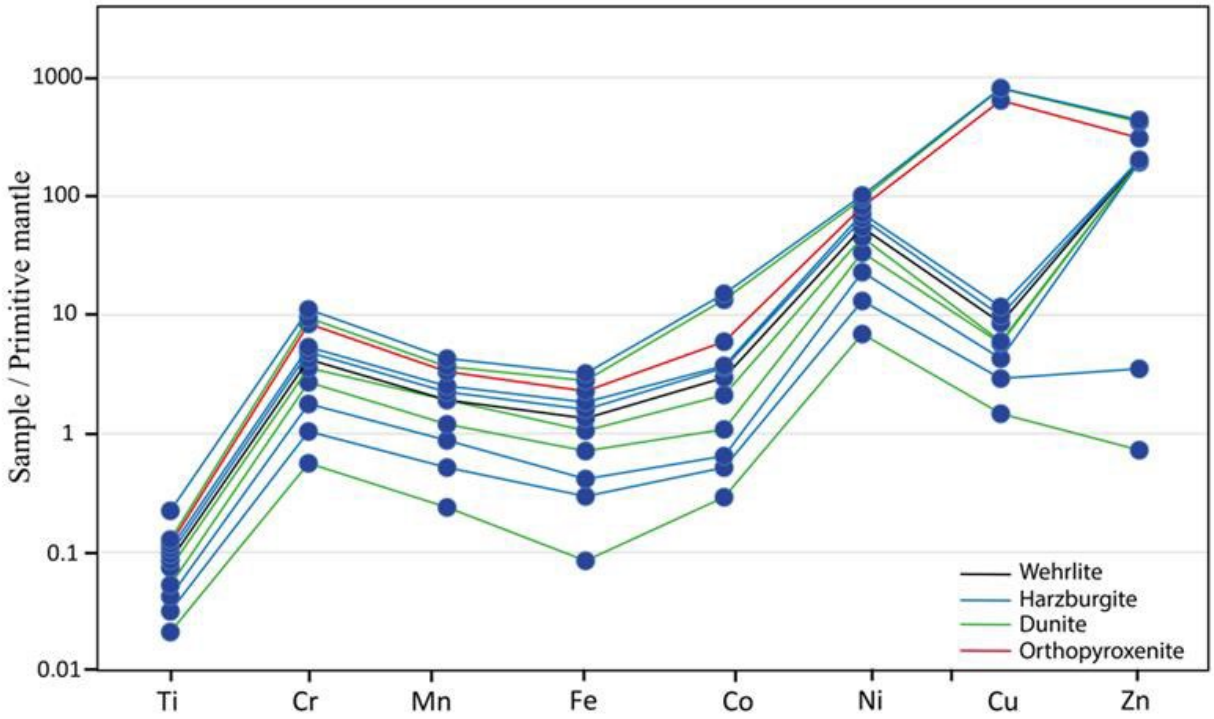

Figure 7. Multi-element spider diagram for the Bou Azzer serpentinites (blue points in all figures), normalized to Primitive Mantle values [48].

5. Discussion

5.1. Preservation of Primary Geochemical Signatures During Serpentinization

The serpentinites of the Bou Azzer ophiolite exhibit relatively high Loss on Ignition (LOI) values, typically ranging from 12.85 to 14.4 wt.% (e.g., samples BMAA 109 and BMAA 105), with specific samples reaching up to 23.67 wt.% (sample BB 20). It is widely recognized that serpentinization processes can significantly increase LOI contents without majorly affecting the primary major element budget [18,49–51]. In Bou Azzer, the observed chemical variations (Figure 8) are primarily interpreted as a reflection of the inherent petrological heterogeneity of the mantle peridotites rather than secondary mobilization [52].

Two distinct groups of serpentinites can be distinguished based on their CaO contents (Figure 8b). Group 1 (0.00–0.98 wt.%) displays CaO levels significantly lower than those of the Primitive Mantle (PM), while Group 2 (1.73–3.77 wt.%) shows concentrations closer to PM values. This distinction is petrologically significant, as higher CaO concentrations correlate with the presence of relict clinopyroxene or the addition of clinopyroxene during refertilization. Although Ca-metasomatism is common near the Co-Ni-As ore deposits, as evidenced by anomalous samples such as BMAA 5a (CaO: 22.06 wt.%), the very low CaO content in the majority of the samples indicates a limited impact of carbonate metasomatism on the bulk geochemistry.

The MgO/SiO_2 ratios (Figure 8a), ranging from 0.81 to 1.12, are consistent with the mean value of 1.02 proposed by [53]. According to this model, serpentinization without brucite formation suggests a process involving minor Mg-loss or SiO_2 gain. Crucially, XRD studies of the Bou Azzer serpentinites did not reveal the presence of brucite [9], suggesting that the pervasive serpentinization involved only minor chemical adjustments. Consequently, we conclude that the major element compositions were effectively conserved during hydration, and the geochemistry of the studied serpentinites reliably reflects the original igneous nature of the mantle protolith. Identification and classification of Bou Azzer serpentinites type and geochemistry is presented in Figures 8–10.

Furthermore, the identification of the mantle protolith is supported by the discrimination diagrams [54]. On the SiO_2–MgO and Al_2O_3–CaO plots (Figure 8a,b), the Bou Azzer serpentinites predominantly cluster within the low-to-high temperature Alpine ultramafic field, showing close affinities with oceanic Mid-Atlantic Ridge peridotites and, for some samples, layered intrusions (Figure 10a,b). This Alpine-type signature is further corroborated by trace element systematics; specifically, the high Ni/Co ratios (Figure 8c) (plotted against Ni) align with the fields of Alpine-type dunite-peridotites [55] As high Ni/Co ratios are characteristic of residues formed during the early stages of mantle partial melting [56], these geochemical proxies collectively confirm that the studied rocks represent refractory mantle fragments rather than crustal cumulates, despite the subtle chemical adjustments induced by seafloor or hydrothermal alteration.

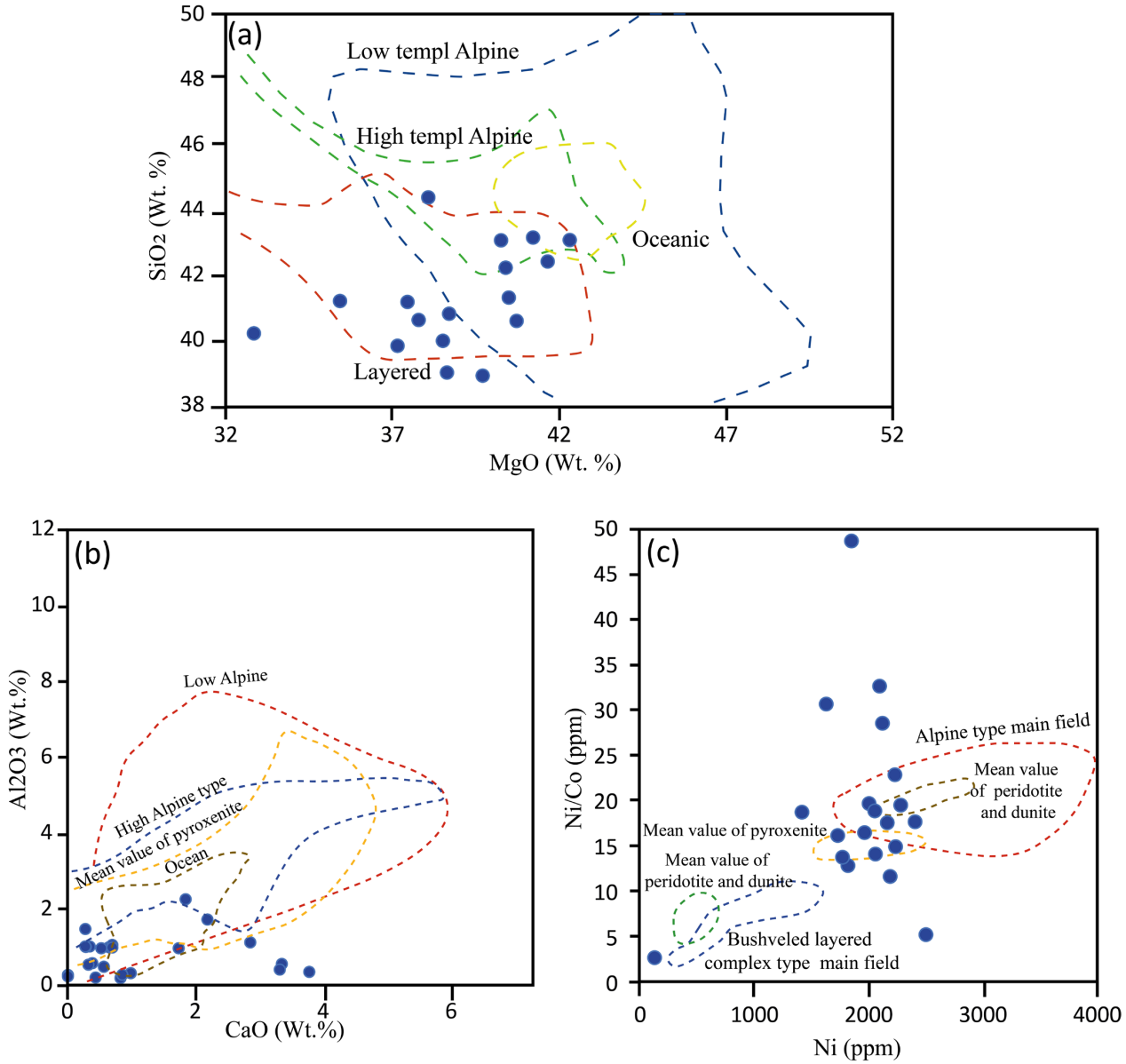

Figure 8. Discrimination and classification diagrams for the Bou Azzer ultramafic rocks: (**a**) SiO_2 versus MgO (wt.%) binary plot after [54] (**b**) Al_2O_3 versus CaO (wt.%) distribution diagram [54], highlighting the contrast between Alpine-type and layered intrusion fields; (**c**) Ni versus Ni/Co ratio plot comparing the studied serpentinites with Alpine-type (dunite-peridotite) and Bushveld-type layered ultramafic complexes (adapted from [57]).

5.2. Mantle Refractoriness and Partial Melting Processes

The MgO concentrations in the Bou Azzer serpentinites (29.46–42.32 wt.%) remain largely unaffected by hydration processes, pointing toward a highly depleted mantle source [22,58,59]. Following the classification of [58], the binary relationship between MgO and H_2O (Figure 9a) reveals a mineralogical assemblage dominated by antigorite, with subordinate lizardite and chrysotile. The predominance of antigorite is indicative of prograde metamorphism, suggesting that these ultramafic units reached significant depths and temperatures during their tectonic evolution.

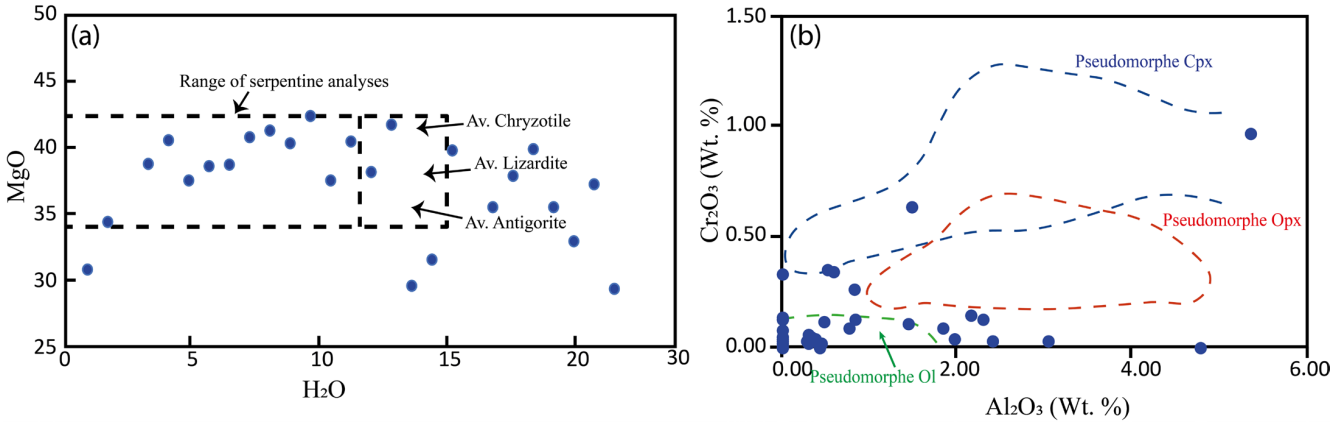

Figure 9. (**a**) MgO vs. H_2O (wt.%) bivariate diagram for the analyzed Bou Azzer serpentinites (modified after [58]]). (**b**) Cr_2O_3 vs. Al_2O_3 (wt.%) plot for serpentines derived from olivine, orthopyroxene, and clinopyroxene; compositional fields are after [60].

Chemical trends in the Cr_2O_3–Al_2O_3 diagram (Figure 9b), consistent with those established by [60], confirm that the serpentine minerals are primarily derived from olivine hydration, with minor contributions from pyroxene. This is chemically summarized by the hydration of olivine (Reaction A) and orthopyroxene (Reaction B), where the absence of brucite, as previously noted, suggests specific silica-saturated conditions during serpentinization.

REACTION A: Global Mixed-Olivine → Serpentine + Magnetite + H_2

$$6(Mg,Fe)_2SiO_4 + 7H_2O \rightarrow 3Mg_3Si_2O_5(OH)_4 + Fe_3O_4 + H_2$$

REACTION B: Orthopyroxene Hydration → Serpentine + Silica

$$3MgSiO_3 + H_2O \rightarrow Mg_3Si_2O_5(OH)_4 + SiO_2$$

According to Bonatti and Michael [61], bulk-rock Al_2O_3 content remains relatively immobile during serpentinization, thus preserving the primary mantle signature. The analyzed Bou Azzer serpentinites (excluding the anomalous BMAA 5a) exhibit Al_2O_3 contents ranging from 0.21 to 2.28 wt.% (Table 1). Their consistently low alkali contents (K_2O: 0.00–0.06 wt.% and Na_2O: 0.00–0.36 wt.%) are typical of depleted peridotites from both modern oceanic settings and ophiolitic massifs [19,20,62–64]. A few samples show localized Na_2O enrichment, likely reflecting the presence of secondary phases such as acmite or relict plagioclase. The lack of correlation between Al_2O_3, CaO, Na_2O, K_2O and the LOI further confirms that these major element distributions are controlled by the protolith mineralogy rather than seafloor weathering or hydrothermal alteration.

The depletion in CaO (0.00–3.92 wt.%, with most samples < 1.0 wt.%) and Al_2O_3 reflects the progressive consumption of clinopyroxene and plagioclase during partial melting. In these harzburgitic residues, Al_2O_3 and CaO contents in excess of the orthopyroxene

contribution (typically 0.6–1.6% Al_2O_3 and 1.3–1.4% CaO [65] are likely hosted in Cr-spinel and exsolved clinopyroxene lamellae. Consequently, samples with slightly higher Al_2O_3 levels (e.g., BB 16, 2.28 wt.%) correspond to a higher modal spinel content or a more fertile (lherzolitic) character, whereas samples like ST 3 (0.21 wt.%) and J 07 (0.00 wt.% CaO) represent highly refractory residues.

The Bou Azzer serpentinites display low Al_2O_3/SiO_2 ratios (mostly < 0.03), which is a key diagnostic feature aligning them with fore-arc mantle wedge serpentinites (Figure 10a). This suggests that their protoliths experienced significant partial melting before serpentinization, a process that leaves these immobile element ratios unaffected [65].

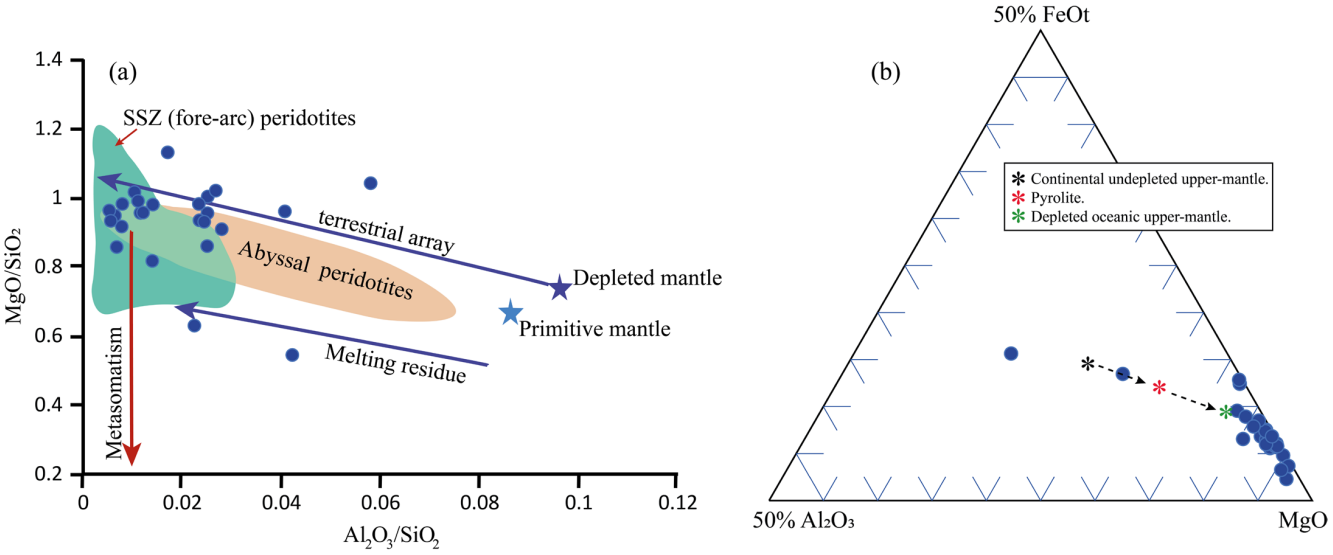

Figure 10. (**a**) MgO/SiO_2 vs. Al_2O_3/SiO_2 bivariate diagram. Primitive and depleted mantle values are from [48] and [66], respectively. The "terrestrial array" represents the bulk silicate Earth (BSE) evolution [67,68]. Abyssal and supra-subduction zone (SSZ) fore-arc peridotite fields are after [17,20,60,62]. (**b**) Ternary MgO-FeO_t-Al_2O_3 diagram (adapted from [61] and references therein) showing the relative abundances of Mg, Fe, and Al in the Bou Azzer serpentinites compared to fertile mantle compositions. Whole-rock data are plotted to illustrate the bulk major-element variation. Arrows indicate the trend of increasing mantle depletion (depletion sequence), reflecting progressive melt extraction from the protoliths.

In the Al_2O_3-FeO-MgO ternary diagram (Figure 10b), the samples follow a clear mantle depletion trend, evolving from a fertile mantle composition toward the MgO-rich apex. While most samples plot as highly refractory residues, the overall chemical variation suggests a transition from mildly depleted lherzolites to highly refractory harzburgites, consistent with the compositional range of ophiolitic mantle sequences.

The whole-rock geochemical signatures of the Bou Azzer serpentinites—notably the extreme depletion in fusible components (Al, Ca, K, Na, P, and Ti) coupled with significant enrichments in compatible elements (Mg, Cr, and Ni)—are classic indicators of a highly refractory mantle residuum. This composition reflects extensive partial melting and the subsequent extraction of basaltic melts. These data suggest that most of the Bou Azzer serpentinites are residual mantle rocks that have undergone variable degrees of melt depletion. The less-depleted domains likely consisted of plagioclase lherzolites, comparable to those observed in the Othrys ophiolite (northern Greece) and other similarly preserved mantle sequences [69].

To further distinguish between a residual mantle origin and magmatic accumulation, the samples were projected onto standard discrimination diagrams (Figure 11). In the AFM space [53] and the Al_2O_3–CaO–MgO ternary diagram [53], the majority of the samples

plot robustly within the metamorphic peridotite and ultramafic tectonite fields, confirming their residual nature (Figure 11a–c). Although a subset of samples exhibits a slight shift toward the ultramafic and mafic cumulate domains—particularly evident in the SiO_2 versus $FeO_t/(FeO_t + MgO)$ diagram (Figure 11d)—this trend does not reflect a primary magmatic origin. Instead, this dispersion is readily explained by the mobilization of major oxides during extensive sub-solidus events, primarily hydration and hydrothermal overprinting.

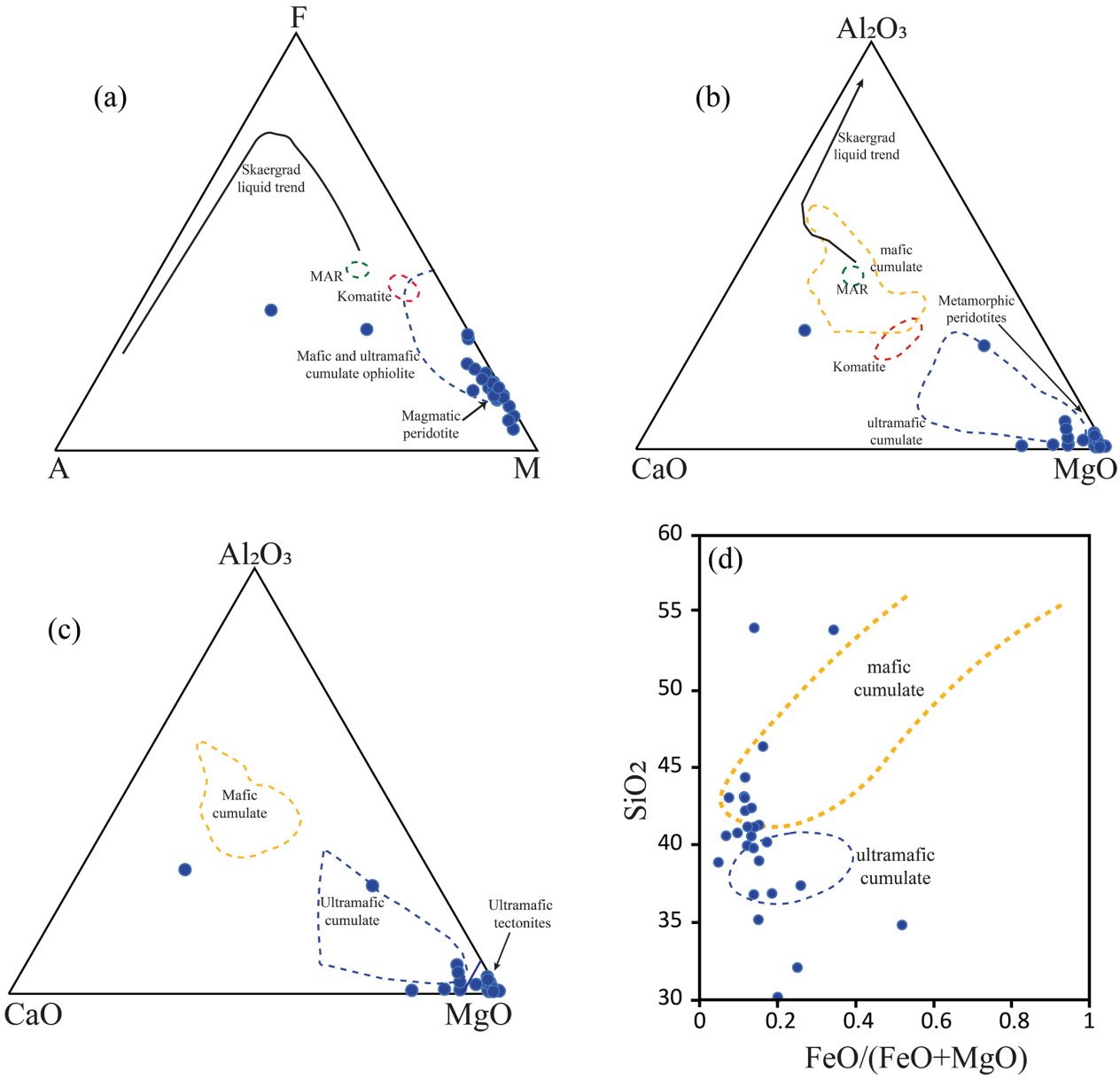

Figure 11. Geochemical discrimination diagrams for the Bou Azzer ultramafic and mafic rocks. (**a**) AFM (ternary diagram (A = Na_2O + K_2O (alkalis)-F = Total FeO (FeO + Fe_2O_3)-(M = MgO (magnésium)) (after Coleman [53]). (**b**) MgO–CaO–Al_2O_3 (wt.%) ternary diagram. The komatiite field is compiled from various sources, and MAR represents the average composition of Mid-Ocean Ridge Basalts. The Skaergaard liquid trend is shown to illustrate the typical differentiation path of basaltic liquids in ophiolite sequences. (**c**) MgO–CaO–Al_2O_3 (wt.%) ternary diagram showing the distribution of the studied samples. (**d**) SiO_2 versus $FeO_t/(FeO_t + MgO)$ variation diagram discriminating ultramafic and mafic cumulates (after Coleman [53]).

5.3. Origin of Lherzolites: Fertile Mantle vs. Refertilization Processes

Based on normative mineral calculations projected onto the standard Ol-Opx-Cpx pseudo-ternary diagram [53] and the SiO_2–CaO–MgO system [70] (Figure 12), the Bou Azzer ultramafic suite is predominantly composed of depleted harzburgites. However, a subordinate subset of samples plots within the lherzolite, wehrlite, and orthopyroxenite fields. The presence of these relatively fertile domains within a highly refractory mantle section raises a critical petrogenetic question: do they represent pristine relics of a fertile mantle, or are they the products of secondary refertilization?

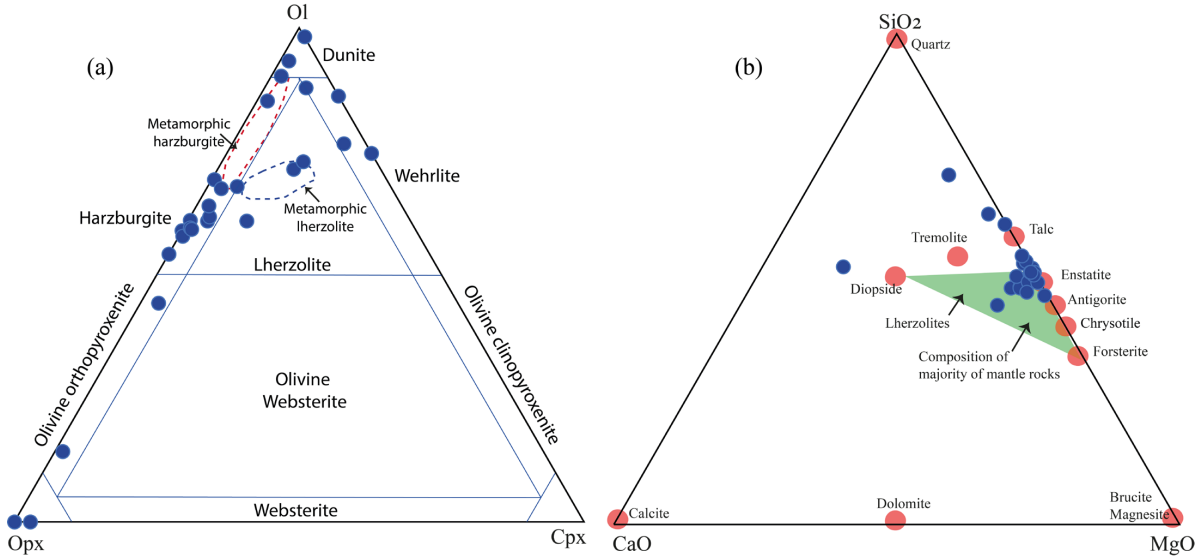

Figure 12. Petrological discrimination diagrams of Bou Azzer serpentinites: (**a**) Modal composition of the studied serpentinites plotted on the Ol–Opx–Cpx classification diagram for peridotites (after Coleman [53]). (**b**) CMS-HC (CaO–MgO–SiO_2) ternary system projected from H_2O and CO_2, illustrating the compositions of rocks and minerals from the Bou Azzer ultramafic unit samples (blue points and red points are stoichiometric minerals, after Bucher & Frey [70]).

The Bou Azzer lherzolitic samples exhibit a paradoxical geochemical fingerprint: they are relatively fertile in terms of major elements (e.g., higher CaO and Al_2O_3) yet remain highly depleted in incompatible trace elements. The noted depletion in incompatible elements eliminates origin from a fertile mantle source and instead suggests partial melting of an already depleted mantle, similar to the depleted Mid-Ocean Ridge Basalt (MORB) mantle [71]. In the Bou Azzer ophiolite, this signature is subsequently modified by slab-derived fluids in a supra-subduction zone environment, enhancing melt extraction and localized refertilization [22,72]. Initially, such a pattern might be interpreted as the residue of the very low-degree partial melting of a fertile peridotitic source, analogous to the Depleted MORB Mantle (DMM) composition. Similar signatures have been described in mantle domains from the southern French Massif Central [73,74].

However, an alternative and more robust model for such orogenic peridotites is the secondary enrichment of a previously refractory mantle. In this scenario, strongly depleted harzburgitic protoliths—which previously underwent 10% to 30% partial melting (Figure 13a)—are subsequently refertilized by the percolation of MORB-like silicate melts or metasomatic fluids [75]. This complex melt–rock interaction is further corroborated by the relationship between modal olivine and bulk-rock Mg# (Figure 13a). The studied samples clearly deviate from simple theoretical partial melting trends, scattering instead along modelled trajectories that are characteristic of reactive porous flow and refertilization processes. This mechanism injects basaltic constituents into the peridotite while preserving

the severe depletion in highly incompatible, magmaphile trace elements. This mechanism is well-documented; for instance, Lenoir et al. (2000) [73] and Puziewicz et al. (2020) [76] demonstrated that LREE-depleted lherzolites from the French Massif Central were generated purely by melt percolation and reaction with a depleted harzburgitic matrix, rather than representing a pristine fertile mantle.

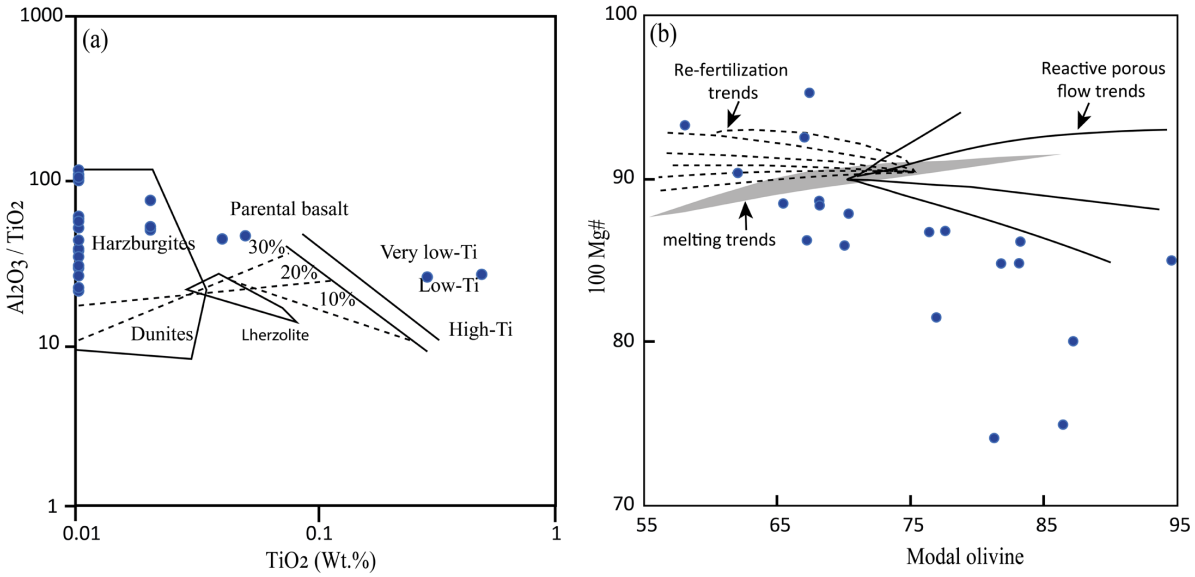

Figure 13. Petrogenetic modeling of the Bou Azzer ultramafic suite. (**a**) Diagram illustrating the genetic relationships (dotted lines) between basaltic melts and their corresponding ultramafic residues, derived from a hypothetical pyrolite mantle source (after Beccaluva et al. 1983 [77]). (**b**) Variation of modal olivine versus bulk-rock Mg# for the Bou Azzer samples. The shaded grey area represents theoretical partial melting trends calculated for various melting reactions within the spinel stability field. Solid curves illustrate reactive porous-flow trajectories, modeled by olivine precipitation coupled with pyroxene dissolution during interaction with infiltrating melts of variable composition (Mg# = 70–80). Dashed curves denote refertilization paths driven by pyroxene-producing reactions. All modeled trends in (**b**) are adapted from Bodinier & Godard (2003) [65].

Applying this framework to the Bou Azzer ophiolite, the localized lherzolitic and wehrlitic compositions most likely capture a complex, two-stage mantle history: an initial profound melt extraction (forming the dominant harzburgites/dunites) followed by partial refertilization via percolating melts (Figure 13b). This multi-stage evolution highlights the highly dynamic nature of the sub-continental lithospheric mantle beneath the Anti-Atlas during the Neoproterozoic, and correlates strongly with processes reported from other major orogenic peridotite massifs.

5.4. Geodynamic Setting

The geochemical and mineralogical signatures of the Bou Azzer peridotites provide robust constraints on their tectonic origin, pointing unequivocally toward a Supra-Subduction Zone (SSZ) environment rather than a typical Mid-Ocean Ridge (MORB) setting. The subarc mantle is defined by its heterogeneity, which is evident in its chemical composition and lithological variability [78,79].

Primary magmatic affinities are well-illustrated using immobile element systematics. In the Cr versus TiO_2 discrimination diagram proposed [80], the analyzed serpentinites predominantly plot within the SSZ ophiolite field (Figure 14a). This is further supported by Al_2O_3/TiO_2 and TiO_2 relationships [77,81], which confirm a highly depleted mantle sequence consistent with Pan-African fore-arc or back-arc basin origins [82]. This subduction-related origin is compellingly reinforced by the redox state of the Bou Azzer

mantle source. The Cr#–ΔlogfO_2 (FMQ) relationship of the constituent chromites demonstrates a trend toward high Cr# and elevated oxygen fugacities relative to MOR peridotites, plotting squarely within the SSZ field for dunites and harzburgites [83] (Figure 14b). As noted by [84,85], variations in fO_2 reflect differences in source chemistry influenced by subduction inputs and redox-active fluids. The Bou Azzer array closely mirrors trends from the Conical and South Sandwich fore-arcs [22], reflecting high degrees of melt extraction followed by oxidizing melt–rock interaction. In this fore-arc to back-arc mantle wedge setting, the infiltration of boninitic or island-arc tholeiitic melts promoted mantle oxidation and subsequent chromite saturation.

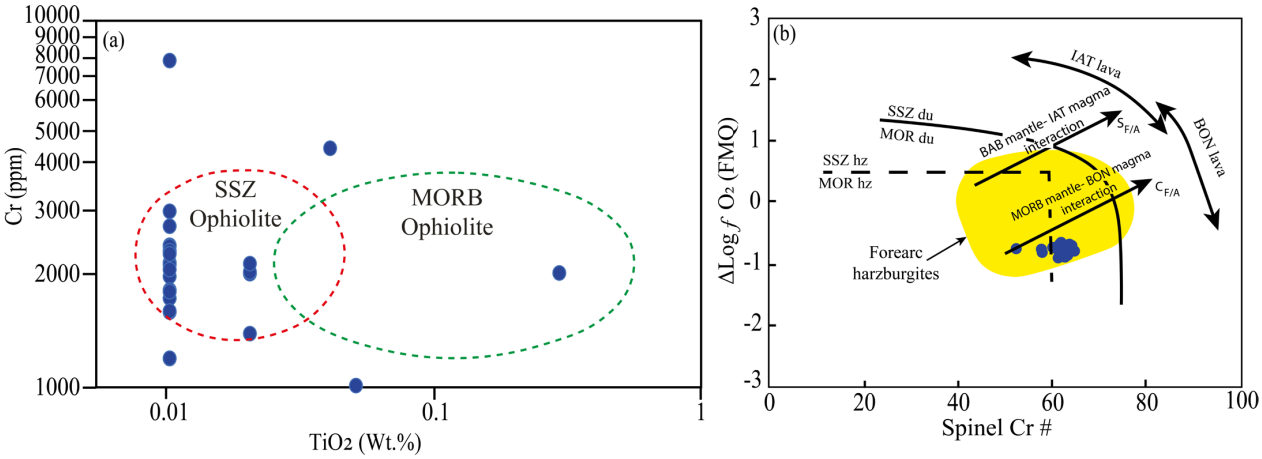

Figure 14. Tectonic discrimination and redox state of the Bou Azzer peridotites. (**a**) Cr versus TiO_2 (wt.%) tectonic discrimination diagram (after [80]), showing the predominant Supra-Subduction Zone (SSZ) affinity of the analyzed serpentinites. (**b**) ΔlogfO_2 (FMQ) versus spinel Cr# for the Bou Azzer peridotites and chromitites, illustrating oxidized SSZ mantle signatures. Oxygen fugacity values were calculated using the olivine–spinel oxybarometer of [86], with temperatures derived from olivine–spinel equilibria following) [87] (see Table 4). MOR–SSZ discrimination fields for dunites (solid line) and harzburgites (dashed line) are shown after [83]. Reference trends defined by peridotites from the Conical Forearc Seamount and the South Sandwich forearc illustrate the interaction between depleted MOR- or back-arc basin–type mantle and supra-subduction zone melts, involving island-arc tholeiitic and boninitic magmatism, respectively [22]. MOR = mid-ocean ridge; SSZ = supra-subduction zone; BAB = back-arc basin; IAT = island-arc tholeiite; BON = boninite.

Trace-element patterns further corroborate this SSZ signature by recording extensive fluid–rock interactions characteristic of subduction channels. While residual serpentinites exhibit extreme Ni enrichment and highly refractory harzburgitic precursors with minimal fluid influence [19,88,89], metasomatized samples display a decoupling between fluid-mobile Large Ion Lithophile Elements (LILE) and High Field Strength Elements (HFSE). The systematic enrichment in Ba and Sr, coupled with localized mobility of Zr and Y, indicates intense modification by sediment-derived, high-temperature fluids typical of subduction and fore-arc environments [18,21]. This selective element mobility reflects varying water-to-rock ratios and highlights how specific subduction fluids (e.g., CO_2- or F-rich) can transport traditionally immobile elements.

Finally, bulk-rock major-element variations using MgO as a proxy for melt extraction (Figure 15) definitively illustrate this progressive evolution. These variations show extreme depletion in basaltic components, approaching compositions expected for residues after 15–25% partial melting [20,90]. Notably, the systematic displacement of these data points toward the Fore-arc Mantle Peridotite (FAP) field [91], which strongly suggests extensive interaction between the depleted peridotites and transient arc-related melts, thereby completing the argument for a dynamic SSZ environment.

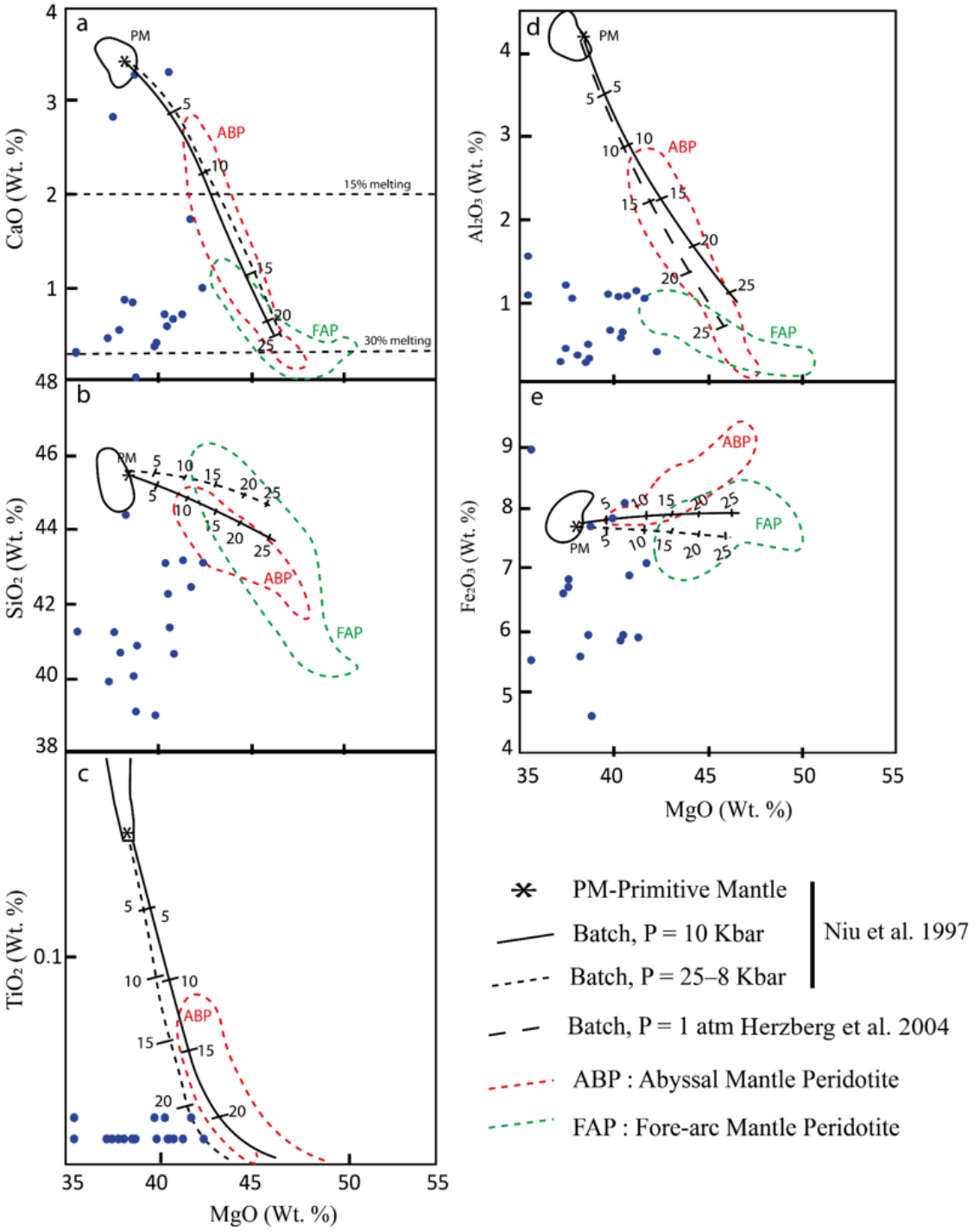

Figure 15. (**a**–**e**) Bulk-rock major-element variation diagrams (wt.%) for the Bou Azzer peridotites, using MgO as an index of melt depletion. The samples display strong depletion in basaltic components, with compositions approaching those expected for refractory residues after ~15–25% partial melting. The data points broadly follow the theoretical melting trends proposed by [20,90]. PM = Primitive Mantle; ABP = Abyssal Mantle Peridotite field; FAP = Fore-arc Mantle Peridotite field (reference fields and trends after [91], and references therein).

However, we emphasize that our estimates of melting degree are not intended to represent absolute values, but rather to provide first-order constraints on the pre-alteration history of the protoliths. By combining bulk composition with olivine-spinel Cr# systematics, we infer that the harzburgitic protoliths underwent moderate prior melting (10–30%), which is consistent with previous studies of supra-subduction fore-arc peri-

dotites [22,75,92]. This approach enables us to reconstruct the multistage evolution of Bou Azzer peridotites: initial depletion via partial melting, followed by serpentinization and metasomatic overprinting.

5.5. Petrogenetic Links Between Mantle Evolution and Podiform Chromitite Formation

Chromite in the Bou Azzer ultramafic suite occurs either as isolated, subhedral to spherical grains surrounded by silicate minerals, or as chain-like aggregates. Skeletal crystals and fine chromite-silicate myrmekitic intergrowths are also observed. Under reflected light, primary chromite appears gray with relatively low reflectivity. However, many grains exhibit a network of undulated or curved fractures displaying a brecciated, fine-dendritic texture.

Consequently, altered chromite rims display a pale gray tone with a faint creamy tinge and higher reflectivity, corresponding to the development of essentially pure magnetite at temperatures below 500 °C [93,94]. Despite these rim alterations, the preserved chromite cores retain their primary magmatic chemistry, as the mobility of trivalent ions is highly restricted up to lower amphibolite-facies conditions [93].

In the Fe^{3+}–Cr^{3+}–Al ternary diagram [95], where samples define a continuous trend from the primary chromian spinel, aluminum–chromite field toward the ferrian (Figure 16a) and from ferrian–pictotite to ferrianchromite (Figure 16b). The most samples plot within alumina chromite. The ferrian–picrochromite compositions of the Bou Azzer chromitites suggest that they formed under highly oxidizing conditions with oxygen fugacity above the FMQ buffer. This process was likely driven by slab-derived fluids [86]. These features are consistent with a supra-subduction zone forearc setting where the interaction between depleted mantle peridotites and boninitic melts promotes chromite crystallization [22]. The Fe^{3+} enrichment suggests overprinting by oxidizing fluids during melt–rock interaction and/or late-stage metasomatism [96]. Taken together, these characteristics support a model involving a depleted mantle, infiltration of boninitic melts, and fluid-induced oxidation, which is typical of SSZ ophiolites, such as the Bou Azzer Ophiolite.

In Figure 16c, chromite compositions are plotted across ophiolitic, stratiform, and komatiitic fields and SE Alaskan-type on the Cr^{3+}–Al^{3+}–(Fe^{3+} + 2Ti) diagram of Jan and Windley [97].

On the Cr_2O_3 and total iron diagram, according to ref. [98] (Figure 16d), it can also be observed that most of the chromite samples analyzed fall within the Alpine-type zone and stratiform type, except for some samples that fall within the Blue Ridge zone, which is widely believed to contain fragments of dismembered ophiolites and alpine-type ultramafic bodies that were incorporated during the Appalachian orogeny (e.g., [99,100]).

This indicates a complex petrogenetic evolution, reflecting variable degrees of mantle depletion, melt–rock interaction, and progressive magma differentiation within a supra-subduction zone environment [55,66,101].

Microprobe analyses of these preserved chromite cores (Table 4) reveal highly refractory compositions characterized by Cr# [Cr/(Cr + Al)] ranging from 0.50 to 0.67, and Mg# [Mg/(Mg + Fe^{2+})] between 0.43 and 0.77. The spinels are notably depleted in minor elements, with $TiO_2 \leq 0.18$ wt.%, MnO ≤ 0.44 wt.%, and NiO ≤ 0.21 wt.%. Statistical evaluation confirms a dominant trend of Cr-rich spinels (~1.7–1.9 apfu) with relatively low Al (0.4–1.0 apfu) and moderate Mg (~0.3–0.5 apfu). This pronounced Cr-enrichment paired with low Al is a classic indicator of chromite crystallization in a Supra-Subduction Zone (SSZ) setting, where high degrees of partial melting expand the Cr-spinel stability field.

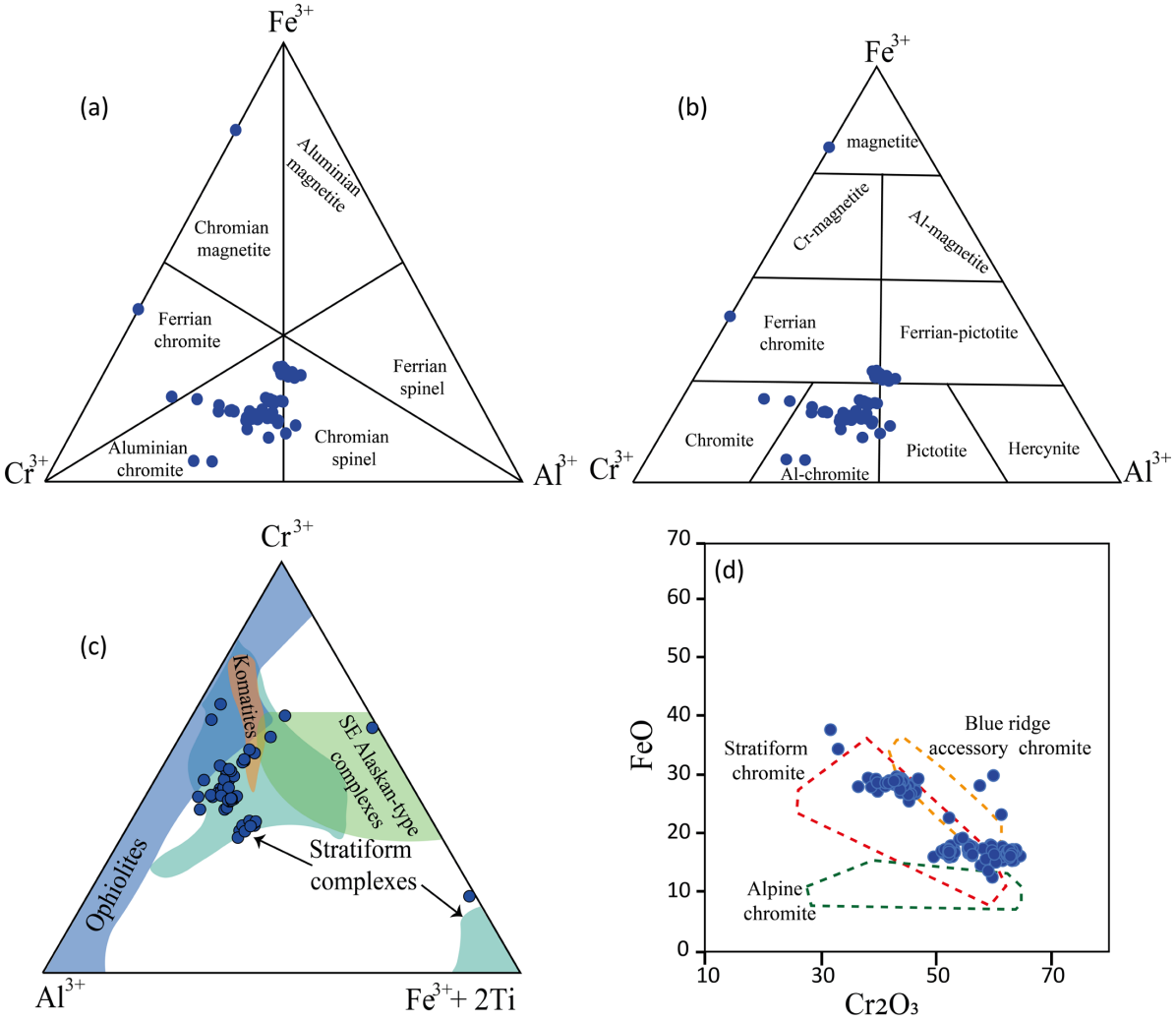

Figure 16. Compositional variations and tectonic discrimination of the Bou Azzer chromites. (**a**) Cr^{3+}–Fe^{3+}–Al^{3+} ternary diagram illustrating the compositional trends of the studied chromites (after Thayer [95]). (**b**) Spinel data from the studied rocks compared with the theoretical stability fields for chromite and magnetite of Sack & Ghiorso [94] (reference diagram after Barnes, 2000 [93]). (**c**) Tectonic discrimination of the studied chromites plotted on the Cr^{3+}–Al^{3+}–(Fe^{3+} + 2Ti) ternary diagram (after ref. [97]). (**d**) Total FeO versus Cr_2O_3 (wt.%) binary diagram for the Bou Azzer chromitites, with reference fields including segregated chromites from the Blue Ridge dunite (after ref. [98]).

Table 4. Composition and structural formulae of the studied chromite samples (calculated based on 32 oxygens). Values represent the proportions in wt.% (Fe, Cr, Al, Mg, Mn) expressed in atoms per formula unit (apfu).

	MgO	SiO_2	TiO_2	V_2O_3	Cr_2O_3	FeO	MnO	NiO	Al_2O_3	CoO	Structural Formulas
Min	9.35	0.20	0.07	0.11	41.13	28.53	0.73	0.19	20.47	0.02	$(Mg_{0.724}Fe^{2+}_{1.238}Mn_{0.032})[Cr_{1.72}Al_{1.27}]O_4$
Max	12.06	0.52	0.16	0.14	60.06	16.31	1.69	0.01	9.84	0.08	$(Mg_{1.09}Fe^{2+}_{0.825}Mn_{0.086})[Cr_{2.4}Al_{0.59}]O_4$
Mean	10.73	0.72	0.07	0.14	52.35	21.19	1.03	0.08	13.00	0.05	$(Mg_{0.76}Fe^{2+}_{1.17}Mn_{0.06})[Cr_{2.18}Al_{0.81}]O_4$

Although some analyzed samples project near the stratiform fields in the Cr^{3+}–Al–Fe^{3+} ternary space [102] (Figure 16c) and the Cr_2O_3 vs. FeO diagram [98] (Figure 16d), their overall geochemical fingerprint confirms an Alpine-type origin. Specifically, the extremely low TiO_2 and MnO concentrations, combined with their association with harzburgite,

dunite, and orthopyroxenite, are definitive hallmarks of podiform chromitites housed in SSZ ophiolites [103,104].

The low TiO_2 content of the parental melt of high-Cr chromitites suggests that the chromitites originated from boninitic melt formed in an island arc environment. In contrast, the parental fluid composition of high-Al chromitites suggests MORB melts as their source.

The MgO/SiO_2 further supports this versus Al_2O_3/SiO_2 systematics of the host serpentinites [68], which define a clear evolutionary trend from abyssal to fore-arc peridotites (Figure 17a).

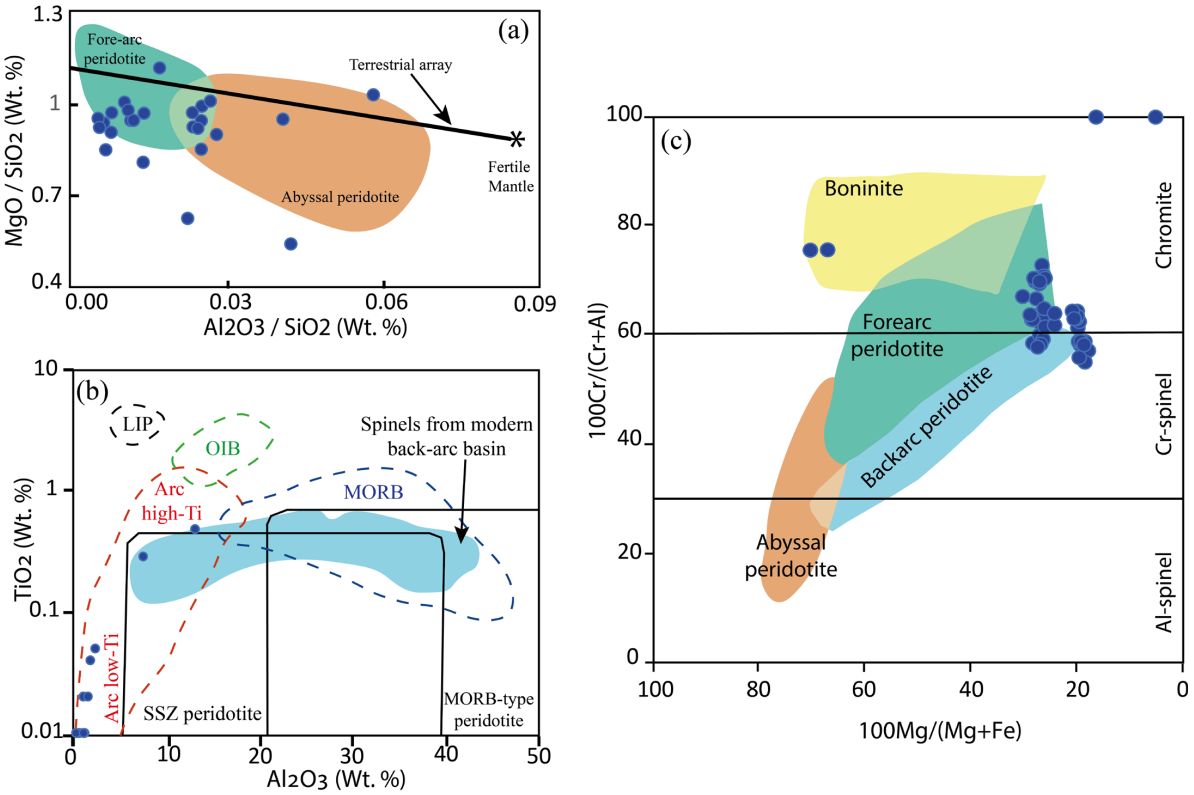

Figure 17. Geochemical and tectonic discrimination diagrams for the Bou Azzer ultramafic suite. (**a**) Bulk-rock MgO/SiO_2 versus Al_2O_3/SiO_2 diagram for the studied serpentinites/peridotites, illustrating the trend from abyssal to fore-arc mantle compositions (reference fields after [105]). (**b**) Primary chromite compositions plotted on the Al_2O_3 versus TiO_2 (wt.%) tectonic discrimination diagram, showing their specific geodynamic affinities (after [106,107] (**c**) Cr# [Cr/(Cr + Al)] versus Mg# [Mg/(Mg + Fe^{2+})] compositional variations in spinels from the Bou Azzer metaperidotites.

The chromitite-bearing ultrabasites of Bou Azzer exhibit low-Ti arc affinities (Figure 17b), which [108] attribute to derivation from a highly depleted mantle wedge heavily fluxed by slab-derived fluids. In the Cr# vs. Mg# compositional space, the Bou Azzer spinels delineate a continuous trend from fore-arc to boninitic back-arc compositions (Figure 17c). Interestingly, while ref. [109] recently proposed a subduction-initiation setting for the Bou Azzer ophiolite, our observed continuous geochemical spectrum, coupled with the extreme major-element depletion of the host peridotites, strongly advocates for a more mature and dynamic SSZ environment.

Using bulk-rock MgO as an index of melt extraction, the peridotites represent refractory residues after ~15–25% partial melting (see Figure 15). While these data closely track the theoretical melting trajectories of [110], the observed scatter—particularly within the Fore-arc Mantle Peridotite field—highlights the crucial role of reactive porous flow. The infiltration of silica-poor, magnesium-rich, and potentially boninitic melts through this

depleted mantle promoted the selective dissolution o+f pyroxenes and the precipitation of olivine. This melt–rock interaction not only reinforced the refractory major-element signatures but also drove the percolating melts toward chromite saturation, resulting in the localized accumulation of podiform chromitites within dunite channels.

Finally, pressure estimates for the Bou Azzer peridotites, ranging from 8 to 25 kbar, provide a coherent physical framework for this model. These pressures correspond to conditions within the shallow lithospheric mantle of a deepening supra-subduction zone, perfectly accommodating the genetic link between deep-seated fluid-fluxed melting, upward reactive melt migration, and the subsequent crystallization of podiform chromitites.

5.6. Tectono-Metamorphic Evolution and Exhumation History

While the primary signatures of the Bou Azzer chromites record an SSZ magmatic origin, their subsolidus modifications provide critical insights into the subsequent tectono-metamorphic evolution of the ophiolite. The observed mineral assemblages and bulk-rock compositions suggest that serpentinization occurred under medium- to high-grade metamorphic conditions, likely associated with hydration processes in a tectonically active subduction environment within the oceanic lithosphere.

On the Al-Cr-Fe stability diagram [94], the studied chromites yield equilibration temperatures higher than 600 °C, plotting far outside the greenschist facies (Figure 18a). In the Cr–Fe^{3+}–Al ternary system (Figure 18b), when compared to the solvus curves and metamorphic facies fields established by [111–114], the Bou Azzer chromites fall far from the greenschist facies, occupying instead the lower amphibolite facies with a distinct trend toward granulite conditions. Chromite compositions exhibit significant dispersion and do not consistently fall within one established metamorphic facies field (Figure 18b). They previously make a trend from lower amphibolite to granulite facies (Figure 18b), and are far from greenschist facies as suggested by ref. [115]. Therefore, chromite compositions are better viewed as indicators of metamorphic grade in the Bou Azzer peridotites.

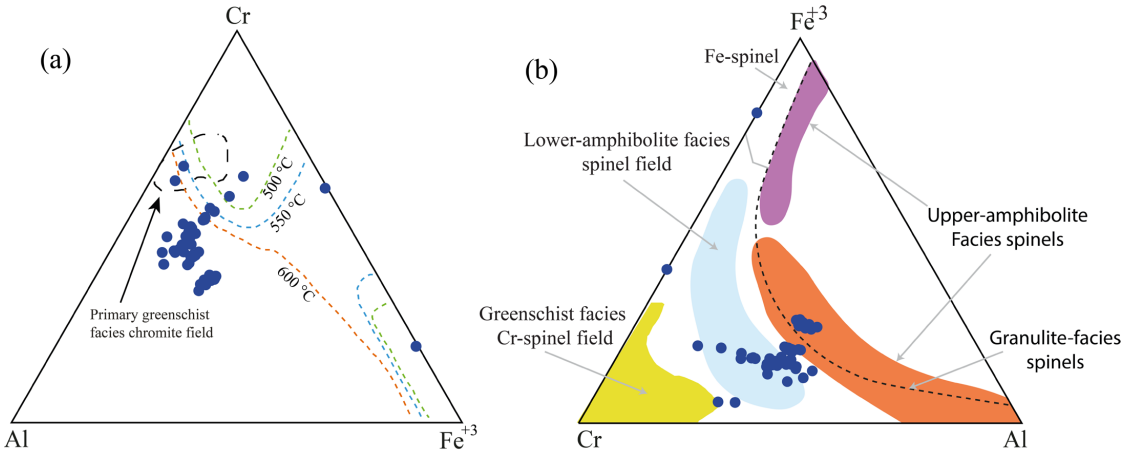

Figure 18. Metamorphic evolution of the Bou Azzer chromites. (**a**) Al-Cr-Fe stability diagram for the studied chromites, indicating equilibration temperatures > 600 °C (reference isotherms and stability fields after rref. [94]). (**b**) Cr–Fe^{3+}–Al ternary diagram. The dashed curve represents the chromite solvus, and the compositional fields corresponding to different metamorphic facies are adapted from refs. [111–114]. The data indicate equilibration in the amphibolite facies, far from greenschist conditions.

This interpretation strongly suggests that the Bou Azzer ophiolite records a high-pressure tectono-metamorphic evolution, and corroborates high-pressure tectono-metamorphic conditions noted in the literature [116–118], challenging models that advocate for the simple obduction of a greenschist-facies sequence [115,119]. The mineralogical and structural characteristics

require deformation and metamorphism under at least amphibolite- to blueschist-facies conditions, implying subduction to significant depths prior to exhumation. Such features distance Bou Azzer from standard Alpine-type ophiolites (e.g., Cyprus or Albania) and align it more closely with classical high-pressure subduction complexes, such as the Franciscan Complex or the Sanbagawa belt, supporting the subduction-accretion models advanced by [114].

5.7. Geodynamic Synthesis and Tectonic Model

The Bou Azzer ophiolite represents a Neoproterozoic supra-subduction zone (SSZ) fragment formed along the northern margin of the West African Craton. Subduction initiation at ca. 760–759 Ma produced a nascent oceanic lithosphere, fore-arc basalts (FABs), and boninites. The infiltration of these arc-related melts into the highly refractory fore-arc mantle promoted intense melt–rock interaction, culminating in the formation of podiform chromitites within a depleted mantle wedge [9,38,44,115,119]. U–Pb zircon ages from the Bou Azzer metagabbros (ca. 759–697 Ma) document this prolonged magmatism, marking the transition from subduction initiation to mature fore-arc development.

Subsequent tectonic extension led to a back-arc environment, characterized by lower degrees of partial melting, localized mantle refertilization, and increased chemical heterogeneity within the peridotites. The ophiolite–mélange association records this complex history, with mélanges documenting the extensive tectonic mixing and accretion that occurred during Pan-African convergence [115].

During final obduction, syn-kinematic arc-related granitoids were emplaced between ca. 659 and 646 Ma [102,120], indicating continued arc activity synchronous with the ophiolite's tectonic emplacement. These granitoids chemically and thermally overprinted the ophiolitic sequence, driving late-stage metasomatism and mineralization. Finally, late-orogenic granitoids (ca. 579 Ma) mark the terminal magmatism following collisional assembly and accretion onto the West African Craton [16,121]. Ultimately, temporal constraints indicate that the Bou Azzer ophiolite preserves a complete Wilson cycle evolution from subduction initiation and fore-arc mantle formation, through back-arc extension, to final obduction and post-collisional granitoid intrusion (Figure 19).

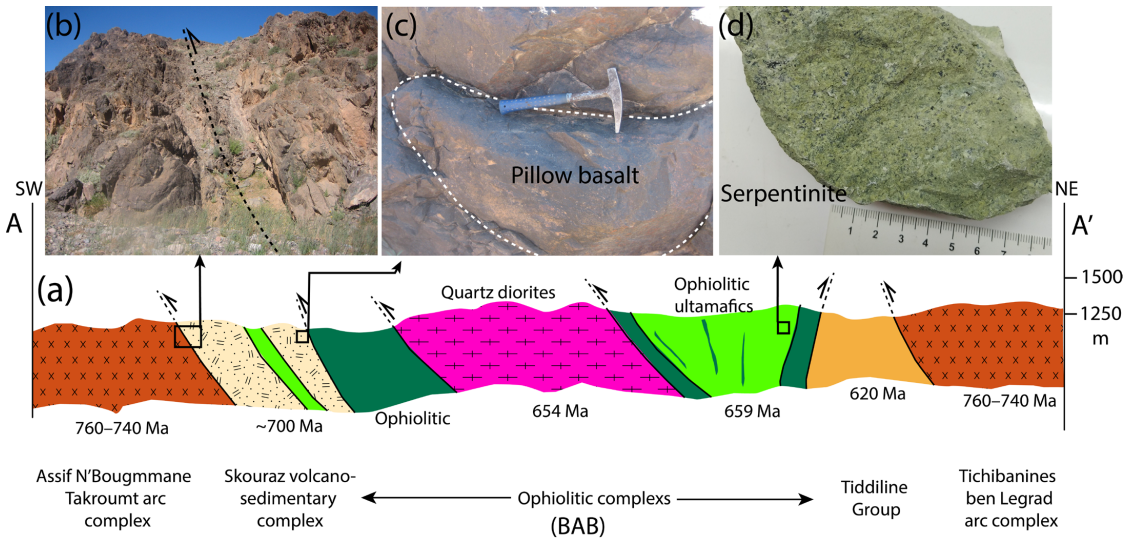

Figure 19. (**a**) SW-NE Interpretative geodynamic cross-section showing the temporal and tectonic evolution of the Bou Azzer ophiolite, from supra-subduction fore-arc development and back-arc extension, to final ophiolite obduction and post-collisional granitoid emplacement. Field details are compiled from [38,39,122,123] (**b**) geological contact between Assif N'Bougmmane Takeroumt arc (SW) and Skouraz volcano-sedimentary complex (NE); (**c**) Pillow lava basalt in the Skouraz volcano-sedimentary complex. (**d**) hand specimen Bou Azzer serpentinite sample.

6. Conclusions

This integrated field, petrographic, mineralogical, and geochemical study of the Bou Azzer ophiolite provides new insights into the complex, multi-stage evolution of a Neoproterozoic supra-subduction zone (SSZ) mantle wedge along the northern margin of the West African Craton. Based on our comprehensive dataset, the main conclusions are as follows:

- Extreme Mantle Depletion and Chromitite Genesis: The mantle sequence is dominated by refractory harzburgitic and dunitic protoliths. Whole-rock geochemistry and chromite mineral chemistry (Cr# = 0.50–0.68; Mg# = 0.43–0.77; extremely low TiO_2) demonstrate that these peridotites are residues of high-degree partial melting (~15–25%). The localized formation of podiform chromitites was driven by intense melt–rock interaction between this highly depleted mantle wedge and infiltrating arc-related (boninitic) melts in a dynamic fore-arc to back-arc setting.
- A Novel High-Pressure Tectono-Metamorphic Record: Challenging previous models that advocate for the simple obduction of a greenschist-facies sequence, thermodynamic and mineral-chemical constraints reveal a much deeper evolution. Serpentinization temperatures exceeding 600 °C, pressure estimates of 8–25 kbar, and the stability of chromite within the lower amphibolite to near-granulite facies strongly indicate that the oceanic lithosphere was subducted to significant depths prior to its exhumation.
- Polyphase Alteration and Metasomatism: The textural evolution of the serpentinites—from high-temperature antigorite to later lizardite and clinochrysotile—records a continuous journey from deep subduction-zone hydration to shallow-level meteoric fluid infiltration. This was accompanied by intense CO_2-rich metasomatism (talc-magnesite alteration) synchronous with the tectonic emplacement of the ophiolite during the Pan-African orogeny.

Ultimately, these findings firmly establish the Bou Azzer ophiolite as a mature, high-pressure SSZ mantle wedge. This study not only refines the geodynamic model for the closure of the Pharusian Ocean but also provides a critical reference for understanding Neoproterozoic mantle melting processes, deep fluid circulation, and the tectono-metamorphic exhumation of ophiolitic complexes along global cratonic margins.

Author Contributions: Conceptualization, methodology, and investigation, A.W.; validation, A.W., Y.A. and A.B.P.; formal analysis, A.W.; resources, A.W. and M.B.M.; writing—original draft preparation, A.W. and R.R.; writing—review and editing, A.W., A.A.L., A.S. (Aref Shirazi), A.S. (Adel Shirazy) and M.B.M.; funding acquisition, A.W. All authors have read and agreed to the published version of the manuscript.

Funding: This research received no external funding.

Data Availability Statement: The data used to support the findings of this study are included within the article.

Acknowledgments: We gratefully acknowledge the support of the Managem Group (Morocco) through the Essential Economic Minerals program, which made this research possible. We also thank the Faculty of Sciences and Technology, University of Lorraine.

Conflicts of Interest: The authors declare no conflicts of interest.

References

1. Dilek, Y.; Furnes, H. Ophiolite Genesis and Global Tectonics: Geochemical and Tectonic Fingerprinting of Ancient Oceanic Lithosphere. *Bull. Geol. Soc. Am.* **2011**, *123*, 387–411. [CrossRef]
2. Pearce, J.A. Immobile Element Fingerprinting of Ophiolites. *Elements* **2014**, *10*, 101–108. [CrossRef]
3. Leblanc, M. *Ophiolites Precambriennes et Gites Arsenies de Cobalt: Bou Azzer (Maroc)*; Centre Géologique et Géophysique: Montpellier, France, 1975.

4. Bodinier, J.L.; Dupuy, C.; Dostal, J. Geochemistry of Precambrian Ophiolites from Bou Azzer, Morocco. *Contrib. Mineral. Petrol.* **1984**, *87*, 43–50. [CrossRef]
5. Naidoo, D.D.; Bloomer, S.H.; Saquaque, A.; Hefferan, K. Geochemistry and Significance of Metavolcanic Rocks from the Bou Azzer-El Graara Ophiolite (Morocco). *Precambrian Res.* **1991**, *53*, 79–97. [CrossRef]
6. Admou, H.; Soulaimani, A.; Mrini, Z. Les Ophiolites Néoprotérozoïques Du Maroc: Témoins de La Tectonique Panafricaine Dans l'Anti-Atlas. In *Geology of Morocco: The Geology of the Maghreb Belts and Tethys Margins*; Springer: Berlin/Heidelberg, Germany, 2013; pp. 277–302.
7. Hefferan, K.; Soulaimani, A.; Samson, S.D.; Admou, H.; Inglis, J.; Saquaque, A.; Latifa, C.; Heywood, N. A Reconsideration of Pan African Orogenic Cycle in the Anti-Atlas Mountains, Morocco. *J. Afr. Earth Sci.* **2014**, *98*, 34–46. [CrossRef]
8. Wafik, A.; Zoheir, B.; Benchekroun, F.; Benaouda, R.; Ben Massoude, M.; Atif, Y.; Beiranvand Pour, A.; Niroomand, S.; El Arbaoui, A.; Karfal, A.; et al. Multistage Gold-Polymetallic Mineralization in the Bou Azzer District, Anti-Atlas, Morocco: Insights from Ore Microscopic, Geochemical, and Fluid Inclusion Studies. *Geofluids* **2024**, *2024*, 5579902. [CrossRef]
9. Wafik, A.; Visalli, R.; Punturo, R.; Conte, A.M.; Guglietta, D.; Ben Massoude, M.; El Aouad, N.; Mabika, N.N.; Cirrincione, R. Neoproterozoic Serpentinites from the Bou Azzer Ophiolite, Central Anti-Atlas (Morocco): Geodynamic Evolution and Mantle Processes beneath the West African Craton Boundaries. *Ital. J. Geosci.* **2025**, *144*, 48–69. [CrossRef]
10. Wafik, A. Etude Géochimique et Métallogénique d'un Système Hydrothermal Océanique Fossile: Exemple Des Minéralisations Cuprifères Dans Les Ophiolites Protérozoïques de l'Anti Atlas Central (Maroc). Ph.D. Thesis, Université Cadi Ayyad, Marrakech, Morocco, 2013.
11. Saquaque, A.; Admou, H.; Cisse, A.; Benyousef, A.; Reuber, I. Les Intrusions Calco-Alcalines de La Boutonniere de Bou Azzer-El Graara (Anti-Atlas, Maroc): Marqueurs de La Deformation Panafricaine Majeure Dans Un Contexte de Collision d'arc. *Comptes Rendus Acad. Des. Sci. Ser. II* **1989**, *308*, 1279–1283.
12. Leblanc, M. The Late Proterozoic Ophiolites of Bou Azzer (Morocco): Evidence for Pan-African Plate Tectonics. *Dev. Precambrian Geol.* **1981**, *4*, 435–451. [CrossRef]
13. Saquaque, A.; Admou, H.; Karson, J.; Hefferan, K.; Reuber, I. Precambrian Accretionary Tectonics in the Bou Azzer-El Graara Region, Anti-Atlas, Morocco. *Geology* **1989**, *17*, 1107. [CrossRef]
14. Leblanc, M.; Lancelot, J.R. Interprétation Géodynamique Du Domaine Pan-Africain (Précambrien Terminal) de l'Anti-Atlas (Maroc) à Partir de Données Géologiques et Géochronologiques. *Can. J. Earth Sci.* **1980**, *17*, 142–155. [CrossRef]
15. Toummite, A.; Liegeois, J.P.; Gasquet, D.; Bruguier, O.; Beraaouz, E.H.; Ikenne, M. Field, Geochemistry and Sr-Nd Isotopes of the Pan-African Granitoids from the Tifnoute Valley (Sirwa, Anti-Atlas, Morocco): A Post-Collisional Event in a Metacratonic Setting. *Mineral. Petrol.* **2013**, *107*, 739–763. [CrossRef]
16. Walsh, G.J.; Benziane, F.; Aleinikoff, J.N.; Harrison, R.W.; Yazidi, A.; Burton, W.C.; Quick, J.E.; Saadane, A. Neoproterozoic Tectonic Evolution of the Jebel Saghro and Bou Azzer—El Graara Inliers, Eastern and Central Anti-Atlas, Morocco. *Precambrian Res.* **2012**, *216–219*, 23–62. [CrossRef]
17. Soulaimani, A.; Ouanaimi, H.; Saddiqi, O.; Baidder, L.; Michard, A. The Anti-Atlas Pan-African Belt (Morocco): Overview and Pending Questions. *Comptes Rendus Geosci.* **2018**, *350*, 279–288. [CrossRef]
18. Deschamps, F.; Godard, M.; Guillot, S.; Hattori, K. Geochemistry of Subduction Zone Serpentinites: A Review. *Lithos* **2013**, *178*, 96–127. [CrossRef]
19. Niu, Y. Bulk-Rock Major and Trace Element Compositions of Abyssal Peridotites: Implications for Mantle Melting, Melt Extraction and Post-Melting Processes Beneath Mid-Ocean Ridges. *J. Petrol.* **2004**, *45*, 2423–2458. [CrossRef]
20. Niu, Y.; Hékinian, R. Spreading-Rate Dependence of the Extent of Mantle Melting beneath Ocean Ridges. *Nature* **1997**, *385*, 326–329. [CrossRef]
21. Kodolányi, J.; Pettke, T.; Spandler, C.; Kamber, B.S.; Gméling, K. Geochemistry of Ocean Floor and Fore-Arc Serpentinites: Constraints on the Ultramafic Input to Subduction Zones. *J. Petrol.* **2012**, *53*, 235–270. [CrossRef]
22. Parkinson, I.J.; Pearce, J.A. Peridotites from the Izu-Bonin-Mariana Forearc (ODP Leg 125): Evidence for Mantle Melting and Melt-Mantle Interaction in a Supra-Subduction Zone Setting. *J. Petrol.* **1998**, *39*, 1577–1618. [CrossRef]
23. Ahmed, A.; Arai, S.; Abdelaziz, Y.; Rahimi, A. Spinel Composition as a Petrogenetic Indicator of the Mantle Section in the Neoproterozoic Bou Azzer Ophiolite, Anti-Atlas, Morocco. *Precambrian Res.* **2005**, *138*, 225–234. [CrossRef]
24. Wafik, A.; Bhilisse, M.; Admou, H.; Maacha, L.; Elghorfi, M. The Podiform Chromite and Platinum Group Elements in the Neoproterozoic Ophiolite Bou Azzer (Inlier Bou Azzer—El Graara, Central Anti-Atlas). *Eur. Sci. J.* **2015**, *11*, 1857–7881.
25. Ionov, D.A.; Hofmann, A.W. NbTa-Rich Mantle Amphiboles and Micas: Implications for Subduction-Related Metasomatic Trace Element Fractionations. *Earth Planet. Sci. Lett.* **1995**, *131*, 341–356. [CrossRef]
26. Pearce, J.A.; Parkinson, I.J. Trace Element Models for Mantle Melting: Application to Volcanic Arc Petrogenesis. *Geol. Soc. Lond. Spec. Publ.* **1993**, *76*, 373–403. [CrossRef]
27. Choubert, G. Histoire Géologique Du Précambrien de l'Anti-Atlas. Ph.D. Thesis, Éditions du Service Géologique du Maroc, Rabat, Morocco, 1963.

28. Leblanc, M. Proterozoic Oceanic Crust at Bou Azzer. *Nature* **1976**, *261*, 34–35. [CrossRef]
29. Gasquet, D.; Ennih, N.; Liégeois, J.P.; Soulaimani, A.; Michard, A. The Pan-African Belt. *Lect. Notes Earth Sci.* **2008**, *116*, 33–64. [CrossRef]
30. Oberthür, T.; Melcher, F.; Saumur, B. Precious and Base Metal Mineralization Associated with Neoproterozoic Ophiolites in the Anti-Atlas, Morocco. *Appl. Earth Sci.* **2009**, *118*, 74–86.
31. Blein, O.; Baudin, T.; Chèvremont, P.; Soulaimani, A.; Admou, H.; Gasquet, P.; Cocherie, A.; Egal, E.; Youbi, N.; Razin, P.; et al. Geochronological Constraints on the Polycyclic Magmatism in the Bou Azzer-El Graara Inlier (Central Anti-Atlas Morocco). *J. Afr. Earth Sci.* **2014**, *99*, 287–306. [CrossRef]
32. Thomas, R.J.; Fekkak, A.; Ennih, N.; Errami, E.; Loughlin, S.C.; Gresse, P.G.; Chevallier, L.P.; Liégeois, J.-P. A New Lithostratigraphic Framework for the Anti-Atlas Orogen, Morocco. *J. Afr. Earth Sci.* **2004**, *39*, 217–226. [CrossRef]
33. Barbey, P.; Oberli, F.; Burg, J.P.; Nachit, H.; Pons, J.; Meier, M. The Paleoproterozoic in Western Anti-Atlas (Morocco): A Clarification. *J. Afr. Earth Sci.* **2004**, *39*, 239–245. [CrossRef]
34. Gasquet, D.; Levresse, G.; Cheilletz, A.; Azizi-Samir, M.R.; Mouttaqi, A. Contribution to a Geodynamic Reconstruction of the Anti-Atlas (Morocco) during Pan-African Times with the Emphasis on Inversion Tectonics and Metallogenic Activity at the Precambrian-Cambrian Transition. *Precambrian Res.* **2005**, *140*, 157–182. [CrossRef]
35. Tuduri, J.; Chauvet, A.; Barbanson, L.; Bourdier, J.-L.; Labriki, M.; Ennaciri, A.; Badra, L.; Dubois, M.; Ennaciri-Leloix, C.; Sizaret, S.; et al. The Jbel Saghro Au(–Ag, Cu) and Ag–Hg Metallogenetic Province: Product of a Long-Lived Ediacaran Tectono-Magmatic Evolution in the Moroccan Anti-Atlas. *Minerals* **2018**, *8*, 592. [CrossRef]
36. Missenard, Y.; Zeyen, H.; Frizon de Lamotte, D.; Leturmy, P.; Petit, C.; Sébrier, M.; Saddiqi, O. Crustal versus Asthenospheric Origin of Relief of the Atlas Mountains of Morocco. *J. Geophys. Res. Solid Earth* **2006**, *111*. [CrossRef]
37. Clauer, N. Géochimie Isotopique Du Strontium Des Milieux Sédimentaires. In *Application à La Géochronologie de La Couverture Du Craton Ouest-Africain*; University of Strasbourg: Strasbourg, France, 1976; Volume 45.
38. Hodel, F.; Triantafyllou, A.; Berger, J.; Macouin, M.; Baele, J.M.; Mattielli, N.; Monnier, C.; Trindade, R.I.F.; Ducea, M.N.; Chatir, A.; et al. The Moroccan Anti-Atlas Ophiolites: Timing and Melting Processes in an Intra-Oceanic Arc-Back-Arc Environment. *Gondwana Res.* **2020**, *86*, 182–202. [CrossRef]
39. Triantafyllou, A.; Berger, J.; Baele, J.M.; Bruguier, O.; Diot, H.; Ennih, N.; Monnier, C.; Plissart, G.; Vandycke, S.; Watlet, A. Intra-Oceanic Arc Growth Driven by Magmatic and Tectonic Processes Recorded in the Neoproterozoic Bougmane Arc Complex (Anti-Atlas, Morocco). *Precambrian Res.* **2018**, *304*, 39–63. [CrossRef]
40. D'Lemos, R.S.; Inglis, J.D.; Samson, S.D. A Newly Discovered Orogenic Event in Morocco: Neoproterozoic Ages for Supposed Eburnean Basement of the Bou Azzer Inlier, Anti-Atlas Mountains. *Precambrian Res.* **2006**, *147*, 65–78. [CrossRef]
41. Michard, A.; Soulaimani, A.; Hoepffner, C.; Ouanaimi, H.; Baidder, L.; Rjimati, E.C.; Saddiqi, O. The South-Western Branch of the Variscan Belt: Evidence from Morocco. *Tectonophysics* **2010**, *492*, 1–24. [CrossRef]
42. Gahlan, H.A.; Arai, S.; Ahmed, A.H.; Ishida, Y.; Abdel-Aziz, Y.M.; Rahimi, A. Origin of Magnetite Veins in Serpentinite from the Late Proterozoic Bou-Azzer Ophiolite, Anti-Atlas, Morocco: An Implication for Mobility of Iron during Serpentinization. *J. Afr. Earth Sci.* **2006**, *46*, 318–330. [CrossRef]
43. Inglis, J.D.; Samson, S.; D'Lemos, R.S.; Admou, H. Timing of Regional Greenschist Facies Deformation in the Bou Azzer Inlier, Anti-Atlas: U–Pb Constraints from Syn-Tectonic Intrusions. In Proceedings of the First Meeting of IGCP 485, El Jadida, Morocco, 4–7 December 2003; pp. 40–42.
44. El Hadi, H.; Simancas, J.F.; Martínez-Poyatos, D.; Azor, A.; Tahiri, A.; Montero, P.; Fanning, C.M.; Bea, F.; González-Lodeiro, F. Structural and Geochronological Constraints on the Evolution of the Bou Azzer Neoproterozoic Ophiolite (Anti-Atlas, Morocco). *Precambrian Res.* **2010**, *182*, 1–14. [CrossRef]
45. Samson, S.D.; Inglis, J.D.; D'Lemos, R.S.; Admou, H.; Blichert-Toft, J.; Hefferan, K. Geochronological, Geochemical, and Nd-Hf Isotopic Constraints on the Origin of Neoproterozoic Plagiogranites in the Tasriwine Ophiolite, Anti-Atlas Orogen, Morocco. *Precambrian Res.* **2004**, *135*, 133–147. [CrossRef]
46. Wafik, A.; Saquaque, A.; El Boukhari, A. Les Chromitites Podiformes et Les Mineraux de Fe-Cu-Ni-Co Associes a l'ophiolite de Bou Azzer-El Graara (Anti-Atlas Central, Maroc). *Ofioliti* **2001**, *26*, 467–478.
47. Schwartz, S.; Guillot, S.; Reynard, B.; Lafay, R.; Debret, B.; Nicollet, C.; Lanari, P.; Auzende, A.L. Pressure-Temperature Estimates of the Lizardite/Antigorite Transition in High Pressure Serpentinites. *Lithos* **2013**, *178*, 197–210. [CrossRef]
48. McDonough, W.F.; Sun, S.S. The Composition of the Earth. *Chem. Geol.* **1995**, *120*, 223–253. [CrossRef]
49. O'Hanley, D.S. *Serpentinites: Records of Tectonic and Petrological History*; Oxford University Press: New York, NY, USA, 1996; ISBN 0195082540.
50. Coleman, R.G. Plate Tectonic Emplacement of Upper Mantle Peridotites along Continental Edges. *J. Geophys. Res.* **1971**, *76*, 1212–1222. [CrossRef]
51. Mével, C. Serpentinisation Des Péridotites Abysales Aux Dorsales Océaniques. *Comptes Rendus Geosci.* **2003**, *335*, 825–852. [CrossRef]

52. Miyashiro, A.; Shido, F.; Ewing, M. Composition and Origin of Serpentinites from the Mid-Atlantic Ridge near 24° and 30° North Latitude. *Contrib. Mineral. Petrol.* **1969**, *23*, 117–127. [CrossRef]
53. Coleman, R.G. *What Is an Ophiolite?* Springer: Berlin/Heidelberg, Germany, 1977; pp. 1–7.
54. Aumento, F.; Loubat, H. The Mid-Atlantic Ridge Near 45° N. XVI. Serpentinized Ultramafic Intrusions. *Can. J. Earth Sci.* **1971**, *8*, 631–663. [CrossRef]
55. Gülaçar, O.F.; Delaloye, M. Geochemistry of Nickel, Cobalt and Copper in Alpine-Type Ultramafic Rocks. *Chem. Geol.* **1976**, *17*, 269–280. [CrossRef]
56. Permingeat, F. Le Gisement de Molybdène, Tungstène et Cuivre d'Azegour (Haut Atlas). Étude Pétrographique et Métallogénique. *Notes M. Sru. Géol Maroc.* **1959**, *141*, 284.
57. Gulacer, R.; Delaoye, M. Étude Géochimique et Pétrologique Des Péridotites Du Bou Azzer (Anti-Atlas, Maroc). *Bull. La Société Géologique Fr.* **1978**, *20*, 567–578.
58. Page, N.J. *Mineralogy and Chemistry of the Serpentine Group Minerals and the Serpent, Nization Process*; The University of California, Berkeley: Berkeley, CA, USA, 1966.
59. Frey, F.A.; John Suen, C.; Stockman, H.W. The Ronda High Temperature Peridotite: Geochemistry and Petrogenesis. *Geochim. Cosmochim. Acta* **1985**, *49*, 2469–2491. [CrossRef]
60. Hébert, R.; Adamson, A.C.; Komor, S.C. Metamorphic Petrology of ODP Leg 109, Hole 670A, Serpentinized Peridotites: Serpentinization Processes at a Slow-Spreading Ridge Environment. In *Proceedings of the Ocean Drilling Program, Scientific Results*; Detrick, R., Honnorez, J., Bryan, W.B., Juteau, T., Robert, S., Honnorez, A., Andrew, C., Garrett, W., Kallryn, M., Gillis, S., Eds.; Ocean Drilling Program: College Station, TX, USA, 1990; Volume 106–109, pp. 103–113. [CrossRef]
61. Bonatti, E.; Michael, P.J. Mantle Peridotites from Continental Rifts to Ocean Basins to Subduction Zones. *Earth Planet. Sci. Lett.* **1989**, *91*, 297–311. [CrossRef]
62. Bé Dard, J.H. Petrogenesis of Boninites from the Betts Cove Ophiolite, Newfoundland, Canada: Identification of Subducted Source Components Downloaded From. *J. Petrol.* **1999**, *40*, 1853–1889. [CrossRef]
63. Godard, M.; Jousselin, D.; Bodinier, J.-L.J.L. Relationships between Geochemistry and Structure beneath a Palaeo-Spreading Centre: A Study of the Mantle Section in the Oman Ophiolite. *Earth Planet. Sci. Lett.* **2000**, *180*, 133–148. [CrossRef]
64. Pearce, J.A.; Barker, P.F.; Edwards, S.J.; Parkinson, I.J.; Leat, P.T. Geochemistry and Tectonic Significance of Peridotites from the South Sandwich Arc–Basin System, South Atlantic. *Contrib. Mineral. Petrol.* **2000**, *139*, 36–53. [CrossRef]
65. Bodinier, J.-L.; Godard, M. Orogenic, Ophiolitic, and Abyssal Peridotites. In *Treatise on Geochemistry*; Holland, H.D., Turekian, K.K., Carlson, R.W., Eds.; Elsevier/Pergamon: Amsterdam, The Netherlands, 2003; Volume 2, pp. 103–170. ISBN 9780080437514.
66. Salters, V.J.M.; Stracke, A. Composition of the Depleted Mantle. *Geochem. Geophys. Geosystems* **2004**, *5*. [CrossRef]
67. Jagoutz, E.; Palme, H.; Baddenhausen, H. The Abundances of Major, Minor and Trace Elements in the Earth's Mantle as Derived from Primitive Ultramafic Nodules. In Proceedings of the 10th Lunar and Planetary Science Conference, Houston, TX, USA, 19–23 March 1979; pp. 2031–2050.
68. Hart, S.R. Heterogeneous Mantle Domains: Signatures, Genesis and Mixing Chronologies. *Earth Planet. Sci. Lett.* **1988**, *90*, 273–296. [CrossRef]
69. Menzies, M.; Allen, C. Plagioclase Lherzolite-Residual Mantle Relationships within Two Eastern Mediterranean Ophiolites. *Contrib. Mineral. Petrol.* **1974**, *45*, 197–213. [CrossRef]
70. Bucher, K.; Frey, M. *Petrogenesis of Metamorphic Rocks*, 6th ed.; Springer: Berlin/Heidelberg, Germany, 1994; ISBN 3-540-57567-7.
71. Workman, R.K.; Hart, S.R. Major and Trace Element Composition of the Depleted MORB Mantle (DMM). *Earth Planet. Sci. Lett.* **2005**, *231*, 53–72. [CrossRef]
72. Kelemen, P.B.; Shimizu, N.; Salters, V.J.M. Extraction of Mid-Ocean-Ridge Basalt from the Upwelling Mantle by Focused Flow of Melt in Dunite Channels. *Nature* **1995**, *375*, 747–753. [CrossRef]
73. Lenoir, X.; Bodinier, J.-L.; Dupuy, C. Contrasting Lithospheric Mantle Domains beneath the Cenozoic Volcanic Centres of the French Massif Central: Evidence from Major and Trace Element Analyses of Peridotite Xenoliths. *Earth Planet. Sci. Lett.* **2000**, *179*, 227–245. [CrossRef]
74. Downes, H.; Reichow, M.K.; Mason, P.R.D.; Beard, A.D.; Thirlwall, M.F. Mantle Domains in the Lithosphere beneath the French Massif Central: Trace Element and Isotopic Evidence from Mantle Clinopyroxenes. *Chem. Geol.* **2003**, *200*, 71–87. [CrossRef]
75. Le Roux, V.; Bodinier, J.-L.; Tommasi, A.; Alard, O.; Dautria, J.-M.; Vauchez, A.; Riches, A.J. V The Lherz Spinel Lherzolite: Refertilized Rather than Pristine Mantle. *Earth Planet. Sci. Lett.* **2007**, *259*, 599–612. [CrossRef]
76. Puziewicz, J.; Matusiak-Małek, M.; Ntaflos, T.; Grégoire, M.; Downes, H. Lithospheric Mantle beneath the Massif Central, France, Preserved in Lithos: Mantle Xenoliths (Spinel Lherzolite Etc.). *Lithos* **2020**, *362–363*, 105467. [CrossRef]
77. Beccaluva, L.; Di Girolamo, P.; Macciotta, G.; Morra, V. Magma Affinities and Fractionation Trends in Ophiolites. *Ofioliti* **1983**, *8*, 307–324.
78. Arai, S.; Hirai, H.; Uto, K. Mantle Peridotite Xenoliths from the Southwest Japan Arc: A Model for the Sub-Arc Upper Mantle Structure and Composition of the Western Pacific Rim. *J. Mineral. Petrol. Sci.* **2000**, *95*, 9–23. [CrossRef]

79. Arai, S.; Abe, N.; Ishimaru, S. Mantle Peridotites from the Western Pacific. *Gondwana Res.* **2007**, *11*, 180–199. [CrossRef]
80. Pearce, J.A.; Harris, N.B.W.; Tindle, A.G. Trace Element Discrimination Diagrams for the Tectonic Interpretation of Granitic Rocks. *J. Petrol.* **1984**, *25*, 956–983. [CrossRef]
81. Pearce, J.A. Statistical Analysis of Major Element Patterns in Basalts. *J. Petrol.* **1976**, *17*, 15–43. [CrossRef]
82. Berhe, S.M. Ophiolites in Northeast and East Africa: Implications for Proterozoic Crustal Growth. *J. Geol. Soc. London.* **1990**, *147*, 41–57. [CrossRef]
83. Dare, S.A.S.; Pearce, J.A.; McDonald, I.; Styles, M.T. Tectonic Discrimination of Peridotites Using FO2–Cr# and Ga–Ti–FeIII Systematics in Chrome–Spinel. *Chem. Geol.* **2009**, *261*, 199–216. [CrossRef]
84. Stolper, E.M.; Newman, S. The Role of Water in the Petrogenesis of Mariana Trough Magmas. *Earth Planet. Sci. Lett.* **1994**, *121*, 293–325. [CrossRef]
85. Kelley, K.A.; Cottrell, E. Water and the Oxidation State of Subduction Zone Magmas. *Science* **2009**, *325*, 605–607. [CrossRef] [PubMed]
86. Ballhaus, C.; Berry, R.F.; Green, D.H. High Pressure Experimental Calibration of the Olivine-Orthopyroxene-Spinel Oxygen Geobarometer: Implications for the Oxidation State of the Upper Mantle. *Contrib. Mineral. Petrol.* **1991**, *107*, 27–40. [CrossRef]
87. Wan, Z.; Coogan, L.A.; Canil, D. Experimental Calibration of Aluminum Partitioning between Olivine and Spinel as a Geothermometer. *Am. Mineral.* **2008**, *93*, 1142–1147. [CrossRef]
88. Arai, S. Characterization of Spinel Peridotites by Olivine-Spinel Compositional Relationships: Review and Interpretation. *Chem. Geol.* **1994**, *113*, 191–204. [CrossRef]
89. Paulick, H.; Bach, W.; Godard, M.; De Hoog, J.C.M.; Suhr, G.; Harvey, J. Geochemistry of Abyssal Peridotites (Mid-Atlantic Ridge, 15°20′N, ODP Leg 209): Implications for Fluid/Rock Interaction in Slow Spreading Environments. *Chem. Geol.* **2006**, *234*, 179–210. [CrossRef]
90. Herzberg, C. Geodynamic Information in Peridotite Petrology. *J. Petrol.* **2004**, *45*, 2507–2530. [CrossRef]
91. Pagé, P.; Barnes, S.-J. Using Trace Elements in Chromites to Constrain the Origin of Podiform Chromitites in the Thetford Mines Ophiolite, Québec, Canada. *Econ. Geol.* **2009**, *104*, 997–1018. [CrossRef]
92. Dilek, Y.; Altunkaynak, Ş. Geochemical and Temporal Evolution of Cenozoic Magmatism in Western Turkey: Mantle Response to Collision, Slab Break-off, and Lithospheric Tearing in an Orogenic Belt. In *Geological Society, London, Special Publications*; Geological Society London Special Publications: London, UK, 2009; Volume 311, pp. 213–233.
93. Barnes, S.J. Chromite in Komatiites, II. Modification during Greenschist to Mid-Amphibolite Facies Metamorphism. *J. Petrol.* **2000**, *41*, 387–409. [CrossRef]
94. Sack, R.O.; Ghiorso, M.S. Chromian Spinels as Petrogenetic Indicators: Thermodynamics and Petrological Applications. *Am. Mineral.* **1991**, *76*, 827–844.
95. Thayer, T.P. Principal Features and Origin of Podiform Chromite Deposits, and Some Observations on the Guleman-Soridag District, Turkey. *Econ. Geol.* **1964**, *59*, 1497–1524. [CrossRef]
96. Scambelluri, M.; Müntener, O.; Ottolini, L.; Pettke, T.T.; Vannucci, R. The Fate of B, Cl and Li in the Subducted Oceanic Mantle and in the Antigorite Breakdown Fluids. *Earth Planet. Sci. Lett.* **2004**, *222*, 217–234. [CrossRef]
97. Jan, M.Q.; Windley, B.F. Chromian Spinel-Silicate Chemistry in Ultramafic Rocks of the Jijal Complex, Northwest Pakistan. *J. Petrol.* **1990**, *31*, 667–715. [CrossRef]
98. Thayer, P.T. Chromite Segregations as Petrogenetic Indicators. *Geol. Soc. S. Afr. Spec. Publ.* **1970**, *1*, 380–390.
99. Hatcher, R.D., Jr. Tectonics of the Southern and Central Appalachian Internides. *Annu. Rev. Earth Planet. Sci.* **1987**, *15*, 337–362. [CrossRef]
100. Misra, K.C.; Keller, F.B. Ultramafic Bodies in the Southern Appalachians: A Review. *Am. J. Sci.* **1978**, *278*, 389–418. [CrossRef]
101. Carswell, D.A. Picritic Magma—Residual Dunite Relationships in Garnet Peridotite at Kalskaret near Tafjord, South Norway. *Contrib. Mineral. Petrol.* **1968**, *19*, 97–124. [CrossRef]
102. Inglis, J.D.; D'Lemos, R.S.; Samson, S.D.; Admou, H. Geochronological Constraints 619 on Late Precambrian Intrusion, Metamorphism, and Tectonism in the Anti-Atlas. *J. Geol.* **2005**, *113*, 39–450. [CrossRef] [PubMed]
103. Allen, C.R. The Petrology of a Portion of the Troodos Plutonic Complex. Ph.D. Thesis, University of Cambridge, Cambridge, UK, 1975.
104. Kröner, A.; Grieling, R.; Reischmann, T.; Hussein, I.M.; Stern, R.J.; Dürr, S.; Krüger, J.; Zimmer, M. Pan-African Crustal Evolution in the Nubian Segment of Northeast Africa. *Proterozic Lithospheric Evol.* **1987**, *17*, 235–257.
105. Hart, S.R.; Zindler, A. In Search of a Bulk-Earth Composition. *Chem. Geol.* **1986**, *57*, 247–267. [CrossRef]
106. Kamenetsky, V.S.; Crawford, A.J.; Meffre, S. Factors Controlling Chemistry of Magmatic Spinel: An Empirical Study of Associated Olivine, Cr-Spinel and Melt Inclusions from Primitive Rocks. *J. Petrol.* **2001**, *42*, 655–671. [CrossRef]
107. Lenaz, D.; Kamenetsky, V.S.; Crawford, A.J.; Princivalle, F. Melt Inclusions in Detrital Spinel from the SE Alps (Italy–Slovenia): A New Approach to Provenance Studies of Sedimentary Basins. *Contrib. Mineral. Petrol.* **2000**, *139*, 748–758. [CrossRef]

108. Ishii, T.; Robinson, P.T.; Maekawa, H.; Fiske, R. Petrological Studies of Peridotites from Diapiric Serpentinite Seamounts in the Izu-Ogasawara-Mariana Forearc, Leg 125. In *Proceedings of the Ocean Drilling Program, Scientific Results*; Fryer, P., Pearce, J.A., Stokking, L.B., Eds.; Ocean Drilling Program: College Station, TX, USA, 1992; Volume 125, pp. 445–485.
109. Pujol-Solà, N.; Proenza, J.A.; Cambeses, A.; Haissen, F.; Escalona-Orellana, H.; Domínguez-Carretero, D.; Ikenne, M.; Maacha, L.; Arenas, R.; Garcia-Casco, A. Petrogenesis of Ultramafic Rocks from the Neoproterozoic Bou Azzer Ophiolite (Morocco): New Insights into a Long-Standing Geodynamic Question. *Int. Geol. Rev.* **2024**, *67*, 830–853. [CrossRef]
110. Niu, Y. Mantle Melting and Melt Extraction Processes beneath Ocean Ridges: Evidence from Abyssal Peridotites. *J. Petrol.* **1997**, *38*, 1047–1074. [CrossRef]
111. Purvis, A.C.; Nesbitt, R.W.; Hallberg, J.A. The Geology of Part of the Carr Boyd Rocks Complex and Its Associated Nickel Mineralization, Western Australia. *Econ. Geol.* **1972**, *67*, 1093–1113. [CrossRef]
112. Evans, B.W.; Frost, B.R. Chrome-Spinel in Progressive Metamorphism—A Preliminary Analysis. *Geochim. Cosmochim. Acta* **1975**, *39*, 959–972. [CrossRef]
113. Suita, M.T.F.; Strieder, A.J. Cr-Spinels from Brazilian Mafic-Ultramafic Complexes: Metamorphic Modifications. *Int. Geol. Rev.* **1996**, *38*, 245–267. [CrossRef]
114. Barnes, S.J.; Roeder, P.L. The Range of Spinel Compositions in Terrestrial Mafic and Ultramafic Rocks. *J. Petrol.* **2001**, *42*, 2279–2302. [CrossRef]
115. Bousquet, R.; El Mamoun, R.; Saddiqi, O.; Goffé, B.; Möller, A.; Madi, A. Mélanges and Ophiolites during the Pan-African Orogeny: The Case of the Bou-Azzer Ophiolitic Suite (Morocco). In *The Boundaries of the West African Craton*; Ennih, N., Liégeois, J.-P., Eds.; Geological Society: London, UK, 2008; Volume 297, pp. 233–247.
116. Hilal, M. *Évolution Tectono-Métamorphique Des Terrains Paléozoïques et Ultramafiques Du Maroc Central*; Université Cadi Ayyad: Marrakech, Morocco, 1992.
117. Hefferan, K.P.; Karson, J.A.; Saquaque, A. Proterozoic Collisional Basins in a Pan-African Suture Zone, Anti-Atlas Mountains, Morocco. *Precambrian Res.* **1992**, *54*, 295–319. [CrossRef]
118. Hefferan, K.P.; Admou, H.; Hilal, R.; Karson, J.A.; Saquaque, A.; Juteau, T.; Bohn, M.M.; Samson, S.D.; Kornprobst, J.M. Proterozoic Blueschist-Bearing Mélange in the Anti-Atlas Mountains, Morocco. *Precambrian Res.* **2002**, *118*, 179–194. [CrossRef]
119. Pujol-Solà, N.; Domínguez-Carretero, D.; Proenza, J.A.; Haissen, F.; Ikenne, M.; González-Jiménez, J.M.; Colás, V.; Maacha, L.; Garcia-Casco, A. The Chromitites of the Neoproterozoic Bou Azzer Ophiolite (Central Anti-Atlas, Morocco) Revisited. *Ore Geol. Rev.* **2021**, *134*, 104166. [CrossRef]
120. Ikenne, M.; Souhassou, M.; Cousens, B.; Montero, P.; Bea, F.; Askkour, F.; Haissen, F.; Beraaouz, E.H.; Ernst, R.E.; Bajddi, A.; et al. Zircon U–Pb Geochronology and Sm–Nd and Rb–Sr Isotope Systematics of Neoproterozoic Granitoïds from Bou Azzer (Anti-Atlas—Morocco): The Obduction Trigger of the Central Anti-Atlas Terrane. *J. Afr. Earth Sci.* **2023**, *202*, 104900. [CrossRef]
121. Inglis, J.D.; MacLean, J.S.; Samson, S.D.; D'Lemos, R.S.; Admou, H.; Hefferan, K. A Precise U-Pb Zircon Age for the Bleïda Granodiorite, Anti-Atlas, Morocco: Implications for the Timing of Deformation and Terrane Assembly in the Eastern Anti-Atlas. *J. Afr. Earth Sci.* **2004**, *39*, 277–283. [CrossRef]
122. Wafik, A.; Massoude, M.B.; Ntarmouchant, N.; Admou, H.; Chatiby, R.; Atif, Y.; Beiranvand Pour, A. Petrological and Geochemical Characteristics of the Skouraz Banded Iron Formation in the Bou Azzer Inlier, Central Anti-Atlas, Morocco: Insights into Geodynamic Implications. *J. Afr. Earth Sci.* **2026**, *236*, 106006. [CrossRef]
123. Abati, J.; Aghzer, A.M.; Gerdes, A.; Ennih, N. Detrital Zircon Ages of Neoproterozoic Sequences of the Moroccan Anti-Atlas Belt. *Precambrian Res.* **2010**, *181*, 115–128. [CrossRef]